Results in Engineering 28 (2025) 108086

Contents lists available at ScienceDirect

Results in Engineering

journal homepage: www.sciencedirect.com/journal/results-in-engineering

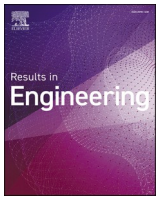

Comprehensive assessment of working fluid selection for ocean thermal energy conversion

Ristiyanto Adiputra [a,*], Rasgianti [b], Ariyana Dwiputra Nugraha [b], Navik Puryantini [a], Gerry Giliant Salamena [c], Aditya Rio Prabowo [d,*]

[a] Research Center for Hydrodynamics Technology, National Research and Innovation Agency (BRIN), Tangerang Selatan, 15310, Indonesia
[b] Power Generation System Research Department, PT PLN (Persero) Research Institute, Jakarta Selatan, 12760, Indonesia
[c] Research Center for Deep Sea, National Research and Innovation Agency (BRIN), Tangerang Selatan, 15310, Indonesia
[d] Department of Mechanical Engineering, Faculty of Engineering, Universitas Sebelas Maret, Surakarta, 57126, Indonesia

ARTICLE INFO

Keywords:
Ocean thermal energy conversion (OTEC)
Working fluid
ASPEN+
Mass and heat balance

ABSTRACT

Ocean Thermal Energy Conversion (OTEC) is a type of ocean renewable energy that generates electricity by utilizing the temperature difference between warm surface seawater and cold deep seawater. Despite its vast potential, especially in tropical regions, OTEC technology remains at the pilot stage. To enhance the implementation of OTEC on a commercial scale, this study aims to determine the working fluid by conducting an in-depth analysis of working fluid selection in OTEC systems, focusing on energy efficiency, safety, and environmental impact. The study involved modeling and creating an in-house program to calculate the heat and mass balance, which was validated using ASPEN+ software in the single-stage Rankine cycle system. The working fluid selection optimization study was conducted through two stages of selection. At the initial stage, the selection involved ten candidate working fluids, based on a literature review of their characteristics, safety, environmental impact, and cost. From the initial selection, four candidates with the highest assessment results were selected, namely Ammonia, R134a, R32, and R22. The second selection stage involved assessing the influence of the four fluids on the quality of power generation and the main equipment specifications for the prospective working fluid. The final results show that Ammonia achieved the highest total score of 37, followed by R32 with a score of 28. In contrast, R22 and R134a scored 23 and 21, respectively.

1. Introduction

Energy saving and carbon dioxide emission reduction have become essential aspects of energy use due to growing concerns about energy shortages, global warming, and environmental pollution [1]. As a result, researchers have extensively investigated ways to utilize renewable and sustainable energy sources more effectively [2], including ocean-based renewable energy such as Ocean Thermal Energy Conversion (OTEC) [3].

Ocean Thermal Energy Conversion (OTEC) converts solar energy stored in tropical and subtropical oceans into electricity [4]. It operates on a Rankine cycle, where a working fluid is vaporized by warm surface seawater and condensed with cold deep water [5,6]. Despite its vast potential and minimal environmental impact, OTEC is limited by low thermal efficiency due to the slight temperature difference between surface and deep seawater [7]. Moreover, some fluids once used in OTEC studies, such as R22, are now phased out under international regulations for their ozone depletion potential (ODP) [8] and are referenced mainly for comparison [9].

Optimization in Ocean Thermal Energy Conversion (OTEC) systems has been widely explored through structural and thermodynamic components. The cold water pipe (CWP) is one of the most studied elements, with research focusing on its structural behavior, internal flow, and performance under marine loading conditions [10–14]. Another critical component is the floating platform, particularly in large-scale OTEC facilities [15]. From a thermodynamic perspective, exergy analysis is commonly applied to identify optimal operating conditions and sensitive components within the cycle. Heat exchangers, especially shell-and-tube types, are central to this process due to their adaptability and simplicity [16–18]. Studies demonstrate that design modifications, such as groove enhancements, can improve heat transfer but may also increase pressure drop, making tube configuration a key optimization

* Corresponding authors.
E-mail addresses: ristiyanto.adiputra@brin.go.id (R. Adiputra), aditya@ft.uns.ac.id (A.R. Prabowo).

https://doi.org/10.1016/j.rineng.2025.108086
Received 19 June 2025; Received in revised form 10 October 2025; Accepted 4 November 2025
Available online 5 November 2025

factor [19–21].

Further research has targeted turbine optimization, where response surface methodology and genetic algorithms have been used to refine variables such as speed, pressure ratio, and blade number [22]. Other studies have also explored the design and optimization of micro radial inflow turbines for low-temperature organic Rankine cycles using preliminary design methods [23]. Integrated hybrid systems combining OTEC with solar, wind, and thermoelectric technologies have also been shown to enhance power generation, freshwater production, and exergy efficiency [24]. In addition, optimization of net power output has highlighted the advantages of the Dual-Pressure Organic Rankine Cycle (DPORC) over the Single-Pressure configuration [25].

Many studies have focused on optimizing various aspects of OTEC system design, yet only a limited number have comprehensively compared different working fluids across multiple criteria. Wang et al. [26] optimized inlet and outlet seawater temperatures using the Multi-Objective Particle Swarm Optimization (MOPSO) algorithm and the LINMAP method. Several working fluids (R717, R600a, R152a, and R134a) were assessed, with R717 showing the best overall performance and R600a exhibiting the highest thermal efficiency—similarly, Sun et al. [27] focused on ammonia and R134a, where net power output was determined by variables such as warm seawater temperature and mass flow rate. The study demonstrated that ammonia is a suitable choice for ORC in OTEC from the perspective of net power output.

Research conducted by Samsuri et al. [28] highlighted the health risks of ammonia and therefore evaluated alternatives such as ammonia–water mixtures, propane, and several refrigerants (R22, R32, R134a, R143a, R410a). Their thermodynamic analysis showed that the ammonia–water mixture provides the highest performance and reliability. Chen et al. [29] further compared six working fluids under uniform conditions, finding that R717 (ammonia) remained the most suitable, with the highest thermal cycle efficiency achieved when turbine inlet and outlet temperatures were fixed. Another study evaluated the impact of temperature on OTEC performance using R717, R600a, R245fa, R152a, and R134a. While ammonia showed relatively lower performance in some aspects, it offered a wider turbine inlet pressure range, which improves operational flexibility [30].

Further analyses categorized organic fluids into wet, dry, and isentropic groups based on parameters such as turbine inlet and outlet conditions, condenser temperature, turbine outlet quality, irreversibility, and overall efficiency. The results show that wet fluids with steep saturated vapor curves provide superior energy conversion, while isentropic fluids achieve high efficiency without requiring regenerators [31]. Related studies on subcritical OTEC cycles further revealed that thermal efficiency is strongly influenced by evaporation and condensation temperatures as well as turbine efficiency, but is less affected by superheating and pump efficiency. R717 was identified as a suitable fluid due to its high thermal efficiency [32].

In OTEC systems, the working fluid plays a central role in capturing heat through the heat exchanger, directly influencing the amount of electricity generated. While many studies have explored OTEC optimization, most have approached fluid selection from a single perspective, focusing either on thermodynamic efficiency, economic feasibility, or environmental impact. However, comprehensive comparisons that integrate these criteria remain limited. To address this gap, the present study emphasizes a multi-criteria assessment of working fluid selection, incorporating energy conversion performance, safety considerations, and environmental sustainability. In doing so, this study contributes by integrating multi-criteria screening with validated cycle modeling and explicitly linking component-level implications to the choice of working fluids for OTEC systems.

2. Methodology

OTEC generates electricity by utilizing the temperature difference in seawater through a thermodynamic cycle, in which the system operates based on mass and heat balance. In this study, the calculation of the mass and heat balance is carried out using the Rankine thermodynamic cycle, as illustrated in Fig. 1, where several calculation parameters must be specifically determined, including seawater characteristics, working fluid enthalpy, pressure drop, pump power requirements, and generator output.

The fluid selection process in this study consists of two main stages:

- Preliminary Assessment – initial screening based on safety, environmental impact, cost, and enthalpy (used only as a scoring indicator); no thermodynamic calculations are performed at this stage.
- Techno-Selection Approach – detailed thermodynamic evaluation of the shortlisted fluids, incorporating enthalpy and other thermodynamic properties, as well as system-level performance indicators.

The blue block represents the Preliminary Assessment, which involves the initial screening of ten candidate working fluids based on enthalpy (see Table 1), safety, environmental impact, and cost considerations as the primary filters. At this stage, enthalpy values are used solely as scoring parameters, where higher values are considered more favorable; however, no thermodynamic performance calculations have been performed yet. This ensures that only fluids meeting minimum safety and sustainability standards, while also showing favorable enthalpy characteristics, are advanced. The process yields a smaller set of fluids suitable for detailed thermodynamic evaluation in the next stage.

The orange block illustrates the Techno-Selection Approach, where the shortlisted fluids are then evaluated using detailed thermodynamic parameters. At this stage, enthalpy and other thermodynamic properties are incorporated, along with their effects on equipment specifications, such as heat exchangers and pumps, as well as on system-level indicators, including capacity factor, efficiency, and annual electricity production. This two-stage approach is designed to reflect a more realistic decision-making process, where screening is performed before detailed performance analysis is conducted.

This stage employs two methods: a numerical simulation using ASPEN Plus and an analytical approach with an in-house code. The results are compared with findings from previous journal studies for validation. Finally, optimization is performed by evaluating power generation performance in parallel with safety, environmental impact, and cost, thereby identifying the most suitable working fluid.

3. Preliminary assessment

3.1. Parameter considerations

Based on a study by Hung et al. [31], it is essential to consider several crucial characteristics of the working fluid, including toxicity, chemical stability, boiling point, flash point, and thermal conductivity. Fluids with low toxicity are used to ensure personnel safety in the event of a leak. The use of chemically stable working fluids is necessary due to the tendency of organic fluids to decompose under high pressure and temperature, which can cause corrosion of surrounding materials. Some organic fluids have extremely low boiling points under standard atmospheric conditions. In such cases, the cooling water temperature in the condenser must be maintained at a very low level, placing additional constraints on the selection of suitable condensers. Furthermore, a working fluid with a high flash point is required to prevent the risk of flammability during operation. High thermal conductivity facilitates more effective heat transfer in the heat exchanger.

The selection of an appropriate working fluid for an OTEC system can be made by determining the system's priority. This priority can be aligned with the characteristics of the working fluid, considering the impact of each property on the system. Several studies highlight key considerations in selecting a working fluid. The evaporation temperature should be lower than the temperature of the surface seawater, while

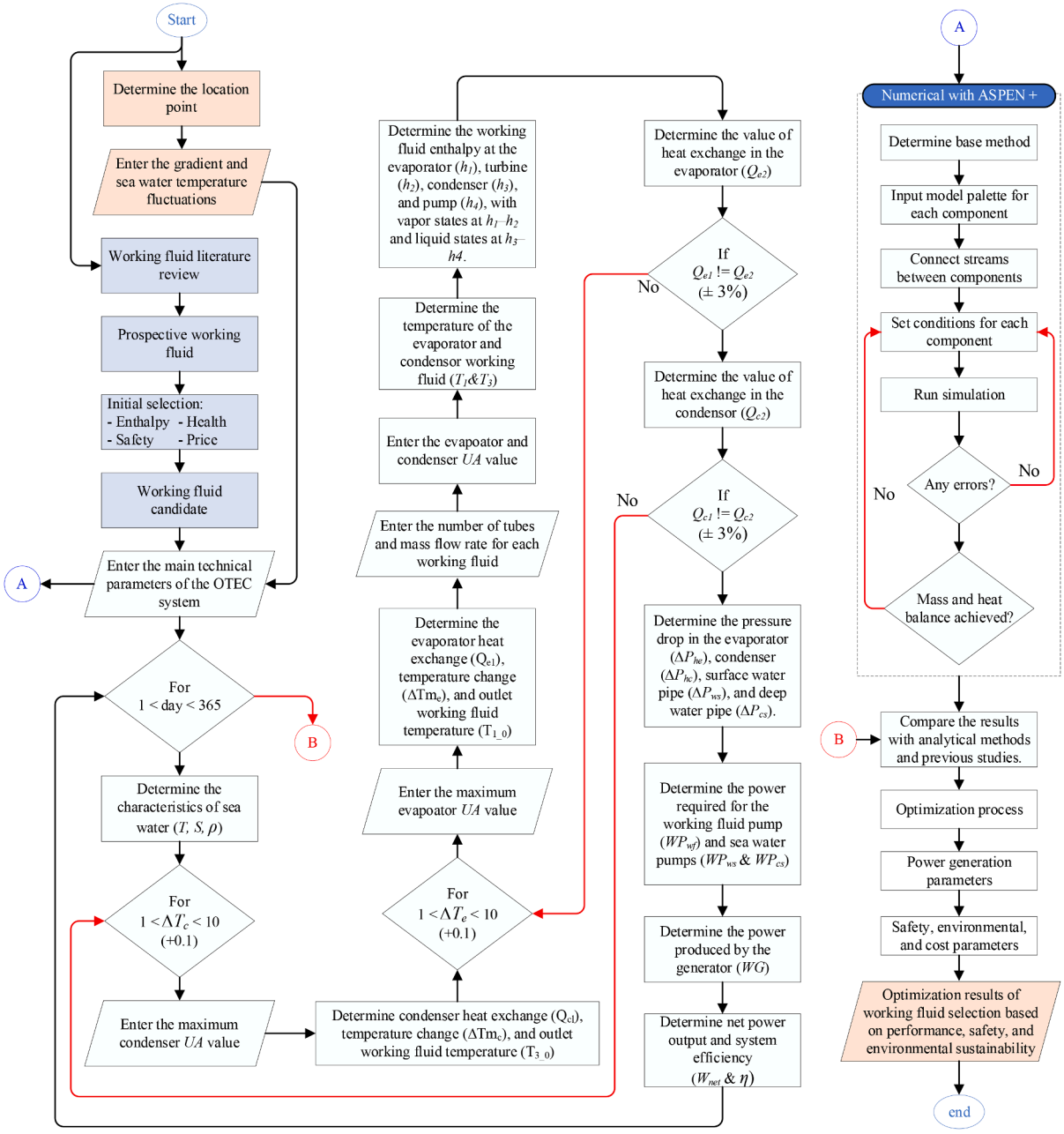

Fig. 1. Flow diagram for working fluid selection in OTEC.

Table 1
Working fluid characteristics.

Parameters	Ammonia	R152a	R134a	R32	R22	R1270	R600a	R290	R744	R245fa
Molecular weight (g/mol)	17.031	66.0	102.032	52.024	86.468	42.090	58.120	44.100	44.0	134.05
Boiling temperature (°C)	−33.33	24.70	−26.30	−51.70	−40,8	−48.00	−11.80	−42.10	−56.60	15.13
Melting temperature (°C)	−77.73	−117.00	−103.30	−136.00	−146.00	−185.00	−159,6	−185.89	−78.50	−102.1
Critical temperature (°C)	132.41	113.50	101.21	78.26	96.30	91.83	134.98	96.70	30.98	154.01
Critical tekanan (Bar)	113.57	45.00	405.93	578.20	499.00	466.43	36.60	42.50	73.77	36.51
Specific Heat (kJ/kg·K)	4.776	1.795	1.421	1.926	1.252	2.659	2.42	2.708	5.77	1.32
Liquid Thermal Conductivity (mW/mK @24 °C)	488.40	98.40	81.60	126.60	84.10	111.20	89.6	94.2	81.5	88.40
Evaporation Enthalpy (kJ/kg, @24 °C)	1169.95	280.57	178.7	272.93	183.73	336.77	330.01	337.49	127.0899	190.91
Evaporation Entropy (kJ/kg-K, @24 °C)	3.9372	0.9442	0.6014	0.9185	0.6386	1.1334	1.1106	1.1357	0.4277	0.6425
ODP	0	0	0	0	0.05	0	0	0	0	0
GWP (AR5)	0	124	1300	675	1760	2	4	3	0	1030
ASHRAE	B2L	A2	A1	A2L	A1	A3	A3	A3	A1	A2

the condensation temperature should be higher than that of the deep seawater. Additionally, the flash point should exceed the temperature of the heat source [33]. The working fluid should not have high operating pressure within the system's temperature range to avoid leakage and improve safety [33]. It should also be inexpensive and easily obtainable, as well as have low toxicity, flammability, explosiveness, and corrosivity [34]. Lastly, it should have zero ozone-depletion potential and a low global warming potential [33].

In the study, ten types of working fluids were selected for analysis, each adjusted to optimize the cycle while considering economic and safety factors. The characteristics of these working fluids are listed in Table 1. The different values of these characteristics yield significant results in the analysis of OTEC system potential and optimization. The use of working fluids with varied parameter values allows for assessing the impact of each parameter. In this selection, besides thermodynamic characteristics, safety factors and global warming potential were also considered.

3.1.1. Enthalpy parameter

One of the primary factors influencing the selection of a working fluid for OTEC systems is its capacity to harness the thermal energy available in seawater. The total energy output is directly proportional to the heat transfer rate within the heat exchanger, which is primarily affected by the enthalpy of the working fluid. A higher enthalpy value indicates a greater ability to absorb heat from seawater, thus enabling the system to generate more power.

As shown in *Fig. 2*, ammonia (R717) exhibits significantly higher enthalpy characteristics compared to the other working fluids analyzed. In contrast, R245fa, R22, and R744 are among the working fluids with the lowest enthalpy values. Notably, the enthalpy of R744 declines sharply above 10 °C, and due to its limited properties, it is only experimentally feasible up to 30 °C. Within this range, its enthalpy remains significantly lower than that of R245fa and R22.

While the energy produced by OTEC is theoretically equivalent to the thermal energy extracted from seawater, several other fluid properties must also be considered when selecting an appropriate working fluid.

3.1.2. Safety parameter

The safety study encompasses several key parameters, including flammability, corrosivity, explosivity, stability, reactivity, and toxicity. Additionally, two classifications are also used: ASHRAE and NFPA (National Fire Protection Association). NFPA Ratings are a chemical safety classification that indicates the level of hazard of a chemical compound. The NFPA rating system provides a numerical scale (0–4) to indicate the hazard level of chemical compounds, with 0 representing non-hazardous substances and 4 indicating extreme danger.

As shown in *Table 2*, all working fluids exhibit low instability, with NFPA instability ratings ranging from 0 to 1. This suggests that they are generally stable and safe for use in OTEC systems. However, differences emerge when health hazards are considered. Among all fluids, ammonia (R717) has the highest health hazard rating of 3, meaning that exposure can cause serious or permanent injury, even with medical treatment. Therefore, strict leak prevention and additional protective measures are essential when using R717. Meanwhile, R134a, R32, R290, R744, and R245fa are rated 2 for health, indicating that prolonged or intense exposure may cause temporary or permanent injury, but risk can be mitigated with prompt handling.

In terms of flammability, R152a, R32, R1270, R600a, and R290 are highly likely to burn even at normal pressure and temperature. Therefore, the OTEC system, which utilizes five working fluids, must be made sterile to prevent widespread fires in the event of a leak. Meanwhile, the other five working fluids, R717/ammonia, R134a, R22, R744, and R245fa, are relatively safe from the possibility of fire because they can only burn at temperatures above 93 °C. According to ASHRAE classification (as shown in Table 3), only R717/ammonia is categorized as having high toxicity. This is consistent with the NFPA rating, which indicates that harmful effects can occur at concentrations below 400 ppm (ppm). The remaining nine working fluids are considered to have

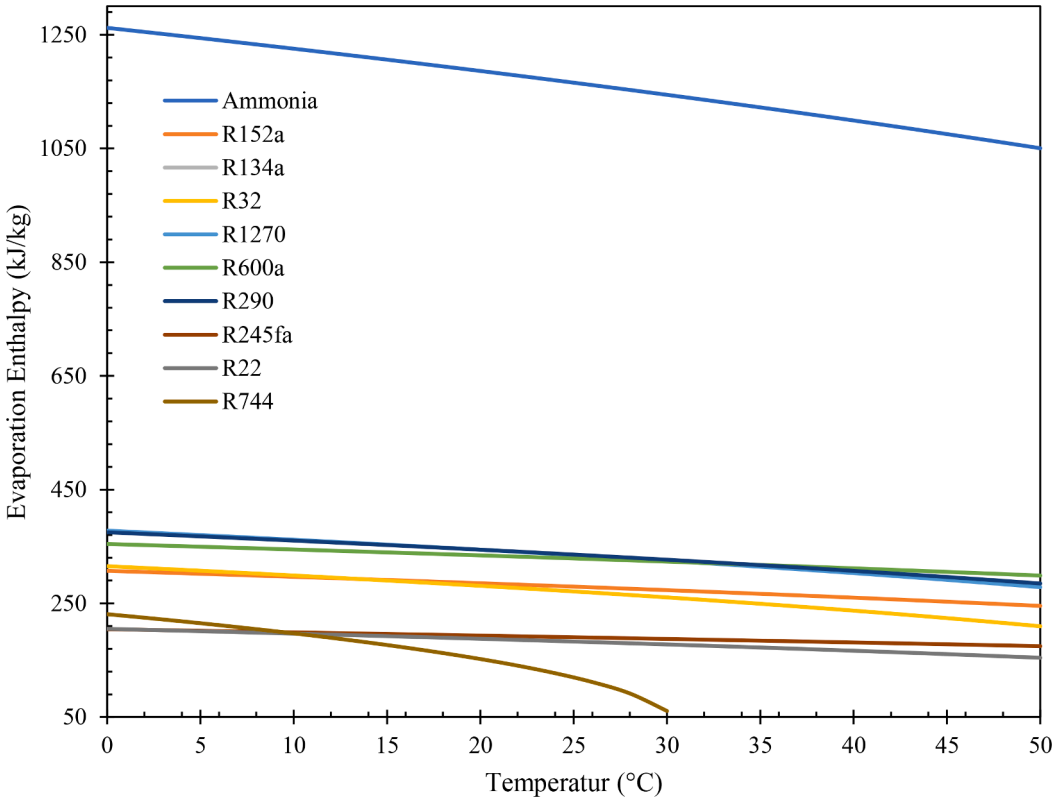

Fig. 2. The relationship between the enthalpy of vaporization and temperature in all working fluids.

Table 2
NFPA rating of each working fluid.

Parameter	Ammonia	R152a	R134a	R32	R22	R1270	R600a	R290	R744	R245fa
Health	3	1	2	2	1	1	1	2	2	2
Flammability	1	4	1	4	0	4	4	4	0	1
Instability	0	1	0	1	1	1	0	0	0	0

Table 3
Working fluid safety parameters.

Parameter	Ammonia	R152a	R134a	R32	R22	R1270	R600a	R290	R744	R245fa
Flammability	Flammable	Very flammable	Not Flammable	Very flammable	Not Flammable	Very flammable	Very flammable	Very flammable	Not Flammable	Not Flammable
Corrosive	Corrosive	Corrosive	Non-Corrosive	Non-Corrosive	Non-Corrosive	Corrosive	Non-Corrosive	Non-Corrosive	Non-Corrosive	Non-Corrosive
Explosivity	High; Auto ignition @669 °C	High; Auto ignition @440 °C	Low; Auto ignition >750 °C	High; Auto ignition @530 °C	Very low	High; Auto ignition @455 °C	High; Auto ignition @460 °C	High; Auto ignition @468 °C	Low	Medium; Auto ignition @412 °C
Stability	Stable	Stable	Stable	Stable	Stable	Stable	Stable	Stable	Stable	Stable
Reactivity	Not reactive	Not reactive	Not reactive	Not reactive	Not reactive	Not Reactive	Not Reactive	Not Reactive	Not Reactive	Not Reactive
Toksisitas	High toxicity	Not toxic	Low toxicity to animals	Low toxicity	Low toxicity	Not toxic	Yes	Not toxic	Not toxic	Not toxic
ASHRAE	B2L	A2	A1	A2L	A1	A3	A3	A3	A1	A2

low toxicity levels. Regarding flammability, R1270, R600a, and R290 are classified as level 3 substances. These fluids demonstrate flame propagation at 60 °C and 101.3 kPa, have a minimum heat of combustion of 19,000 kJ/kg, and a maximum lower flammability limit (LFL) of 0.10 kg/m³.

3.1.3. Health parameter

The use of working fluids with high levels of atmospheric contamination contradicts the environmental objectives of OTEC systems. Greenhouse gases contribute to global warming by absorbing thermal energy and preventing its release into the atmosphere. In this study, the Global Warming Potential (GWP) is used as a metric to compare the capacity of different working fluids to trap heat, with carbon dioxide (CO_2) serving as the reference standard, under IPCC guidelines. As shown in Fig. 3, working fluids such as R22 and R134a have a GWP above 1000, so they are not environmentally friendly in the context of global warming. As long as they do not leak, they can still be used in OTEC systems. In contrast, R717/ammonia has a GWP of zero and does not absorb or release energy into the atmosphere.

Ozone Depletion Potential (ODP) is a relative index that compares the ability of a compound to deplete ozone with that of CFC-11, which is assigned a value of 1. Among the ten working fluids considered, almost all exhibit an ODP of zero, except for R22, which has a relatively low value of 0.05. While this is acknowledged in the literature by Zhang et al. [31], it is essential to note that this value is an order of magnitude lower than that of typical CFCs and thus represents a significantly smaller contribution to ozone depletion. Furthermore, in the context of OTEC applications, the working fluids operate in a closed-loop cycle with negligible emissions to the atmosphere, which significantly reduces environmental risks compared to conventional refrigeration systems. Therefore, the inclusion of R22 in the preliminary screening remains scientifically justifiable, as its ODP impact under OTEC operational

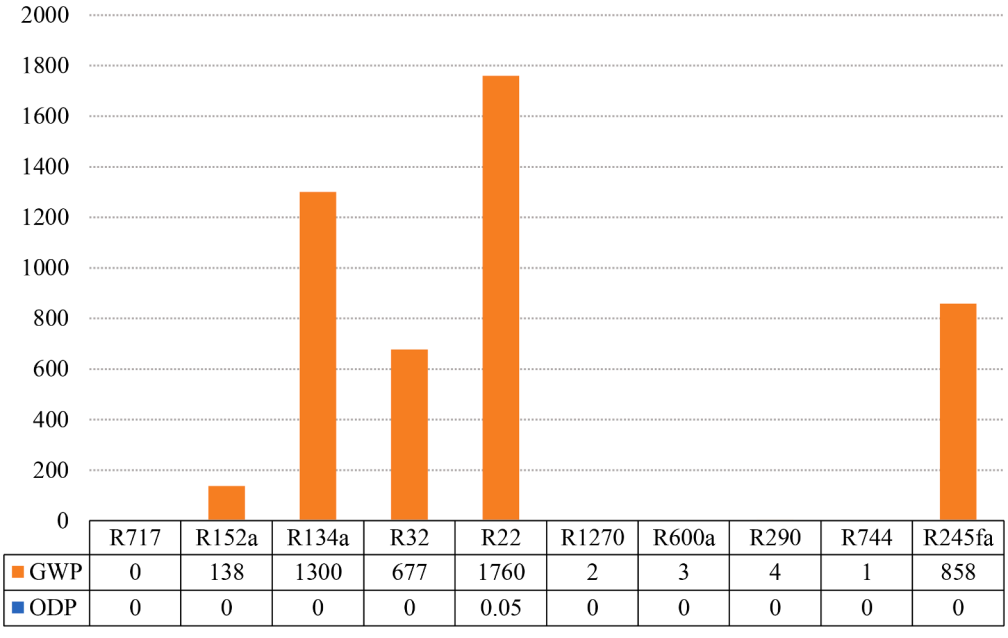

	R717	R152a	R134a	R32	R22	R1270	R600a	R290	R744	R245fa
GWP	0	138	1300	677	1760	2	3	4	1	858
ODP	0	0	0	0	0.05	0	0	0	0	0

Fig. 3. Potential parameters of working fluids that contribute to global warming.

conditions is marginal compared to its thermodynamic relevance.

3.1.4. Cost parameter

As shown in Table 4, R152a has the lowest cost per metric ton (MT) among the evaluated working fluids. However, its cost does not differ significantly from that of most other fluids. The most significant cost disparities are observed with R1270 and R245fa, which exhibit the highest price variation within the group.

3.2. Screening method

To ensure a transparent and structured evaluation, each parameter in the screening method was assigned a score based on its relative influence on key performance indicators of the OTEC system. The indicators considered include Annual Energy Production (AEP), Capacity Factor (CF), and Environmental Impact, with each parameter scored on a 0–5 scale (0 = no influence, 5 = highly influential). This scoring framework facilitates a balanced comparison by highlighting the most critical factors for thermodynamic performance and economic feasibility, while also considering potential safety and health impacts under abnormal operating conditions. The weighting of each parameter reflects its relative impact on energy production and environmental considerations, with higher scores assigned to factors that are directly related to these aspects. The detailed scoring matrix is presented in Table 5.

Enthalpy received the highest score for AEP and a high score for CF because it directly governs the thermodynamic efficiency of the OTEC cycle [35,36]. A higher enthalpy difference between the warm and cold seawater streams allows greater energy extraction, which translates into improved net power output and system performance [37]. However, it was scored zero for environmental impact, since enthalpy itself does not cause direct environmental consequences. Its role is strictly technical, confined to influencing the energy conversion process without affecting external ecological or health-related aspects. Cost plays a dominant role in determining the economic feasibility of OTEC. It was scored highest for CF since cost directly affects the ability of the system to operate competitively and sustainably at scale [38]. It also has a significant influence on AEP, as financial limitations may constrain the system design and operational efficiency [38]. Its effect on environmental impact is moderate, primarily through material choices and lifecycle considerations [39]. Overall, cost is a critical driver for evaluating whether an OTEC plant can be realistically implemented.

Safety and Health were both scored zero for AEP and CF, as they do not directly affect energy output or operational reliability under normal operating conditions. However, both parameters were assigned the maximum score for environmental impact because their relevance becomes critical under abnormal scenarios, such as leakage of working fluid, structural failures, or accidental exposure [40]. In such cases, potential risks may involve not only environmental contamination but also hazards to operators and nearby communities [41]. While these risks can be mitigated through proper engineering design, safety standards, and containment procedures [42].

In summary, the technical analysis highlights that enthalpy plays the most dominant role in determining OTEC system performance, as it directly governs thermodynamic efficiency and net energy production. Cost also significantly influences both capacity factor and annual energy production, making it a crucial factor in determining the feasibility of large-scale deployment. By contrast, safety and health do not significantly impact performance metrics under normal operations but become highly relevant in failure scenarios, such as working-fluid leakage or structural damage, which may pose risks to the environment and nearby communities. For this reason, the scoring method prioritizes enthalpy and cost as the primary determinants of OTEC feasibility, while safety and health are considered essential safeguards for environmental and social sustainability

Given this prioritization, the next step is to translate the scoring framework into the selection of working fluids. In particular, enthalpy is treated as a primary technical criterion, alongside environmental considerations such as global warming potential. The scoring of working fluids based on enthalpy is derived from Table 1, using a scale from 1 to 5. As shown in Table 5, each score corresponds to a specific enthalpy range: a value of 1 represents 100–200 kJ/kg, while a value of 5 means 500 kJ/kg and above (∞). The enthalpy values used in this assessment refer to the evaporation enthalpy of each fluid at a constant temperature of 24 °C. This temperature was selected because it is commonly reached by working fluids in typical OTEC operations.

To evaluate the impact of working fluids on global warming, a maximum score of 5 is used, based on their Global Warming Potential (GWP). The classification of scores and corresponding GWP ranges is also presented in Table 6. In terms of cost, the scoring ranges from 1 to 5, depending on whether the price is above or below $1000 and whether the fluid is domestically available. Cost is considered a significant factor, as it can substantially affect the overall value and feasibility of the system.

The standard used to assess the safety and health parameters of working fluids is presented in Table 7. Safety is evaluated based on flammability levels according to the ASHRAE classification, while health risks are assessed based on toxicity, also following the ASHRAE classification. Both parameters are evaluated using a scoring scale from 1 to 4. For the safety parameter, the classification is divided into two main categories: fluids with an ASHRAE flammability classification of 2 are assigned a score of 2. In contrast, those with a classification of 2 L are assigned a score of 3.

3.3. Initial selection results

The assessment of a working fluid is based on four main points: enthalpy, safety, health, and cost. All of these points have varying maximum values, depending on their level of importance. Parameters with high importance, such as enthalpy capacity and cost, are given a maximum value of 5. Other parameters, such as safety and health, are given a maximum value of 4.

Table 4
Cost of working fluid.

Working fluid	Cost (MT)	Working fluid	Cost (MT)
Ammonia	$ 502.00	R1270	$ 2550.00
R152a	$ 450.00	R600a	$ 461.00
R134a	$ 750.00	R290	$ 600.00
R32	$ 480.00	R744	$ 505.00
R22	$ 526.00	R245fa	$ 3100.00

Table 5
Scoring of key parameters for OTEC working fluid selection.

Parameter	Annual Energy Production (AEP)	Capacity Factor (CF)	Environmental Impact
Enthalpy	5	4	0
Cost	4	5	3
Safety	0	0	5
Health	0	0	5

Table 6
Basis for assessing the enthalpy and global warming threat parameters of working fluids.

Value	Range	
	Enthalpy	GWP
1	100 – 200	1000 – ∞
2	200 – 300	750 – 1000
3	300 – 400	500 – 750
4	400 – 500	250 – 500
5	500 – ∞	0 – 250

Table 7
Basic assessment of safety and health parameters of working fluids.

Value	Flammability	Toxicity
1	3	B
2	2	
3	2L	A
4	1	

Table 8
Working fluid assessment results.

Working Fluid	Parameters				Total
	Enthalpy	Safety	Health	Cost	
Ammonia	5	2	2	5	14
R152a	2	2	4	4	12
R134a	1	4	4	4	13
R32	2	3	4	4	13
R22	1	4	4	4	13
R1270	3	1	4	3	11
R600a	3	1	4	4	12
R290	3	1	4	4	12
R744	1	2	4	5	12
R245fa	1	4	4	3	11

Based on the preliminary assessment results for each working fluid listed in Table 8, it is found that the working fluid with the best value is R717 or ammonia. The working fluids with the lowest values are R1270 and R245fa. Although the ammonia working fluid has an average value in four parameters, the value of 5 in the enthalpy and cost parameters makes ammonia have the highest total value.

In terms of safety and health, the majority of working fluids receive a safety score of 4, indicating they are either non-flammable or have low flammability. Ammonia is the only fluid with both a high flammability level and an ASHRAE B toxicity classification. Furthermore, when the safety and health parameter scores are combined, only ammonia has a total value below 5. This stands in stark contrast to its enthalpy score, which reaches the maximum point of 5 based on a single assessment parameter. Conversely, only ammonia and R744 attain a score of 5 in the cost parameter. When selecting the four most suitable working fluids, aside from ammonia, the other three with high total scores are R134a, R32, and R22. These fluids each have a total value of 13, although their enthalpy scores range only from 1 to 2. The relatively low enthalpy values of these fluids should be given more attention, as enthalpy is a key parameter that determines the power output of an OTEC system.

In terms of safety and health, ammonia (R717) shows a notably lower score compared to the other three candidates. For both parameters, it only receives a score of 2, while the others generally receive a score of 4. Given the significant differences among these four fluids across the three primary parameters, a more comprehensive evaluation is necessary to determine the most suitable working fluid for OTEC systems. In terms of safety and health, the majority of working fluids receive a safety score of 4, indicating they are either non-flammable or have low flammability. Ammonia is the only fluid with both a high flammability level and an ASHRAE B toxicity classification. Furthermore, when the safety and health parameter scores are combined, only ammonia has a total value below 5. This stands in stark contrast to its enthalpy score, which reaches the maximum point of 5 based on a single assessment parameter. Conversely, only ammonia and R744 attain a score of 5 in the cost parameter.

When selecting the four most suitable working fluids, aside from ammonia, the other three with high total scores are R134a, R32, and R22. These fluids each have a total value of 13, although their enthalpy scores range only from 1 to 2. The relatively low enthalpy values of R134a (178.7 kJ/kg) and R22 (184.73 kJ/kg) are compensated by their good safety and cost scores. At the same time, R32 achieves the exact total due to a balance between moderate enthalpy and favourable cost. The relatively low enthalpy values of these fluids should be given more attention, as enthalpy is a key parameter that determines the power output of an OTEC system. In terms of safety and health, ammonia (R717) shows a notably lower score compared to the other three candidates. For both parameters, it only receives a score of 2, while the others generally receive a score of 4. These contrasting characteristics explain why ammonia leads overall, as its very high enthalpy (1169.95 kJ/kg) and low cost outweigh its safety and health drawbacks. In contrast, the other fluids rely more on their safer and less toxic profiles to remain competitive. Given the significant differences among these four fluids across the three primary parameters, a more comprehensive evaluation is necessary to determine the most suitable working fluid for OTEC systems.

4. Techno selection approach

Based on the selection and initial assessment of ten working fluids, the four best working fluids were ammonia, R22, R32, and R134a. The OTEC system is planned to have a capacity of 100 kW, assuming a power plant electricity demand of 20 %. Therefore, the optimization of the 100 kW OTEC system must be able to achieve the 120 kW target.

In the optimization of OTEC systems, it is essential to define the limitations and general assumptions related to system components [39]. Establishing these assumptions is necessary to enable a fair comparison of the performance of the four working fluids. In addition to the power generation capacity, several other system components are standardized. This standardization encompasses key components, including the generator, turbine, pump, heat exchanger, and seawater pipeline.

One approach to standardizing components is by applying uniform efficiency values. As shown in Table 9, two types of efficiency values are presented: reference-based efficiency and the efficiency used in calculations. The efficiency used in calculations is 10 % lower than the reference value. This reduction acts as a safety factor, based on the assumption that the actual performance of components in the constructed OTEC system may be lower than that in the referenced systems.

In addition to efficiency, component uniformity is also ensured by the basic size of components, such as pipes and heat exchangers. The uniformity of the seawater pipe components is carried out with the assumption that each working fluid system uses the same type and size of pipe. Additionally, the seawater pipe is assumed to be installed in an inclined position, with a uniform distance and depth between each working fluid system. As for the heat exchanger, since its performance will be affected by the type of working fluid, uniformity is applied to the tube size and basic design. The uniformity of the seawater pipe and heat exchanger components is listed in Table 10.

In addition to component uniformity, the same case configuration is used to optimize the generating system. In this optimization, it is assumed that the power plant is located on land, with the seawater intake located approximately 2 km from the Ambon Bay shoreline in Indonesia. The average temperature at depths of 30 m and 400 m is obtained as shown in Table 11.

OTEC System Calculation Method

The calculation of the power generated by the OTEC system is based on the heat equilibrium of the system. In the Rankine Cycle, there are three approaches to determining the heat exchange during the cycle. The heat exchange calculation is formulated in Eqs. (1)–3 for the

Table 9
Main component efficiency parameters.

Parameter	Value		References
	References	Used	
Generator efficiency (%)	95	85	[43]
Turbine efficiency (%)	95	85	[43]
Working fluid pump efficiency (%)	85	75	[44]
Sea water pump efficiency (%)	85	75	[44]

Table 10
Parameters of heat exchangers and seawater pipes.

Parameter	Value
Heat exchanger length (m)	8
Tube inner diameter (mm)	9
Tube thickness (mm)	0.7
Number of passes	6
Tube pitch	1.25 × Tube outer diameter
Tube material	Titanium
Distance between Baffles (m)	0.5
Pitch Layout	Triangular
Sea water pipe diameter (m)	1
Sea water pipe material	HDPE
Length of surface seawater pipe (m)	2138
Length of deep-sea water pipe (m)	105

Table 11
Parameters of temperature and average salinity of seawater.

Parameter	Value
Temperature at 30 m Depth (°C)	28.62
Temperature at 400 m Depth (°C)	8.013
Salinity at 30 m Depth (ppt)	33.772
Salinity at 400 m Depth (ppt)	34.492

evaporator and Eqs. (4)–6 for the condenser.

$$Q_e = m_{WF}(h_1 - h_4) \tag{1}$$

$$Q_e = UA(\Delta Tm_e) \tag{2}$$

$$Q_e = m_{WS}c_{P,WS}(T_{wsi} - T_{wso}) \tag{3}$$

$$Q_c = m_{WF}(h_2 - h_3) \tag{4}$$

$$Q_c = UA(\Delta Tm_c) \tag{5}$$

$$Q_c = m_{CS}c_{P,CS}(T_{cso} - T_{csi}) \tag{6}$$

Where $Q_{e,c}$ is the heat flow rate in the evaporator and condenser (kW), m_{WF} is the mass flow rate of the working fluid (kg/s), $m_{CS,WS}$ is the mass flow rate of surface and depth seawater (kg/s), h is the enthalpy of the working fluid at each point (kJ/kg), $c_{P,WS,CS}$ is the specific heat of surface and depth seawater (kJ/(kg.K)), $\Delta Tm_{e,c}$ is the temperature change in the evaporator and condenser (K), $T_{csi,o}$ is the cold seawater temperature at the condenser inlet and outlet (K), $T_{wsi,o}$ is the warm seawater temperature at the condenser inlet and outlet (K), U is the heat exchange coefficient of the heat exchanger (kW/(m^2.K)), and A is the total heat exchange area of the heat exchanger (m^2).

The heat exchange between seawater and the working fluid in the heat exchanger is strongly influenced by the input and output temperatures of the two fluids [45]. As shown in Fig. 1, the change in seawater temperature after passing through the heat exchanger is assumed in the loop. The working fluid temperature after going through the evaporator and condenser (T_1 and T_3) is calculated twice, using the UA minimum target, and after the UA actual calculation. The working fluid temperature in the heat exchanger is determined by Eqs. (8) and 9

$$T_{wso,cso} = T_{wsi,csi} \pm \Delta T_{e,c} \tag{7}$$

$$T_1 = \frac{e^{\left[\frac{T_{wsi}-T_{wso}}{\Delta Tm_e}\right]}T_{wso} - T_{wsi}}{e^{\left[\frac{T_{wsi}-T_{wso}}{\Delta Tm_e}\right]} - 1} \tag{8}$$

$$T_3 = \frac{e^{\left[\frac{T_{cso}-T_{csi}}{\Delta Tm_c}\right]}T_{cso} - T_{csi}}{e^{\left[\frac{T_{cso}-T_{csi}}{\Delta Tm_c}\right]} - 1} \tag{9}$$

Where $\Delta T_{e,c}$ is a change in seawater temperature after going through the evaporator and condenser (K) and $T_{1,3}$ is the working fluid temperature after going through the evaporator and condenser (K).

Immediately after going through the heat exchanger, the condition of the working fluid is assumed to be in a pure saturated condition, where the evaporator is in a saturated vapor condition, and the saturated liquid is in the condenser. So that the enthalpy of the working fluid in the evaporator (h_1) and condenser (h_3) is determined by adjusting the temperature and pressure to the specific enthalpy of the working fluid. As illustrated in Fig. 4, the enthalpy value in the turbine and condenser exhibits a deviation from the pure saturated line. Therefore, it is necessary to calculate this value separately, as outlined in Eqs. (10)–13 for turbines and Eqs. (14)–16 for working fluid pumps.

$$s_1 = s_{2i} \tag{10}$$

$$x_{2i} = \left(s_2^{'} - s_{2i}\right)/\left(s_2^{'} - s_3\right) \tag{11}$$

$$h_{2i} = x_{2i}h_2^{'} + (1 - x_{2i})h_3 \tag{12}$$

$$h_2 = h_1 - (h_1 - h_{2i})\eta_T \tag{13}$$

$$P_4 = P_1 \tag{14}$$

$$h_{4i} = h_3 + v_3(P_4 - P_3) \tag{15}$$

$$h_4 = h_3 + \frac{(h_{4i} - h_3)}{\eta_{P,WF}} \tag{16}$$

Where s is entropy (kJ), P is pressure (kPa), v is the specific volume of the working fluid (m^3), η_T is turbine efficiency, and $\eta_{P,WF}$ is working fluid pump efficiency.

The calculation of the heat exchange coefficient and the total heat exchange area of the heat exchanger is based on the assumption that the heat exchanger in use is of the shell-and-tube type. The primary heat exchange occurs between the seawater and the working fluid. The working fluid is consistently located within the tube section, both in the evaporator and the condenser. Conversely, the seawater is always situated within the shell section.

The turbulence of seawater flow within the shell will significantly impact the efficiency of heat exchange within the heat exchanger. The

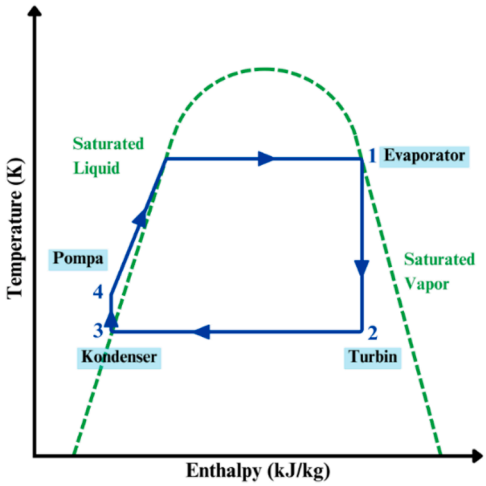

Fig. 4. Temperature-enthalpy diagram of the OTEC rankine cycle.

greater the turbulence, the more effective the heat exchange. In the design, the shell section is equipped with a barrier in the form of baffles, which directs seawater and increases turbulence within the flow. Accordingly, the mass flow rate of seawater in the shell section is determined by Eq. (17), wherein the seawater flow area (A_S) is influenced by the shell diameter (D_s), number of tubes (N), distance between tubes (C), distance of baffles (B), and distance between tubes/pitches (p_t), as listed in Eqs. (18)–21.

$$G_S = \frac{m_{CS.WS}}{A_S} \tag{17}$$

$$A_S = \frac{D_s C B}{p_t} \tag{18}$$

$$C = p_t - d_{ot} \tag{19}$$

$$D_b = d_{ot}\left(\frac{N_t}{k}\right)^{1/n} \tag{20}$$

$$D_s = D_b + C \tag{21}$$

Where $m_{CS.WS}$ is seawater mass flow rate (kg/s), A_S is the area of seawater flow on the shell (m^2), D_s is shell diameter (m), B is the distance between baffles (m), C is clearance [$p_t - d_{ot}$], p_t is the distance between tubes (m) [1.25 $\times$ d_{ot}], D_b is the diameter of the tube assembly (m), N_t is the number of tubes, and d_{ot} is the outer diameter of the tube (m).

The convection coefficient of seawater (h_{SW}) is represented using the Nusselt Number (Nu_{sw}). Nusselt numbers are the ratio of convection to conduction heat transfer in a fluid. The greater the Russell number, the greater the heat transfer that occurs. Where the Nusselt number value is determined by the Reynolds number ($Re_{h.sw}$) as a representation of the ratio of flow conditions and the Prandtl number (Pr_{sw}) as a representation of the thermal diffusivity ratio of seawater.

$$h_{SW} = \frac{Nu.k_{sw}}{D_e} \tag{22}$$

$$Nu_{sw} = 0.047 {Re_{h.sw}}^{0.8} Pr^{1/3} \tag{23}$$

$$Re_{h.sw} = \frac{D_s \times G_s}{\mu} \tag{24}$$

$$Pr_{sw} = \frac{\mu c_{p.sw}}{k_{sw}} \tag{25}$$

$$D_e = \frac{4\left({p_t}^2 - \pi\frac{{d_o}^2}{4}\right)}{\pi d_{ot}} \tag{26}$$

Where k_{sw} is thermal conductivity of sea water (kW/(m.K)), μ is dynamic viscosity (kg/ms), and D_e is equivalent shell diameter (m).

In contrast to the seawater flow within the shell, which is constrained by baffles, the fluid flow within the tube is relatively undisturbed by obstacles. This is due to the small diameter of the tube used, which precludes the possibility of adding grooves. Furthermore, tubes that have many grooves will result in a notable pressure drop. The mass flow rate of the working fluid in each tube will decrease in proportion to the number of tubes, as demonstrated by Eqs. (27) and 28. Consequently, although there is an increase in the heat transfer area, the number of tubes does not necessarily correlate with an increase in heat transfer in the heat exchanger.

$$G_t = \frac{m_{WF}}{A_t} \tag{27}$$

$$A_t = N_t\frac{a_t^{'}}{n} \tag{28}$$

Where m_{WF} is working fluid mass flow rate (kg/s), $a_t^{'}$is the flow area in each tube (m^2), and n is the number of passes.

As in the shell section, the working fluid convection coefficient (h_{WF}) in the tube is also described by the Nusselt Number (Nu_{wf}). However, different from the shell section, the Nusselt number on the tube is calculated depending on the Reynolds number ($Re_{h.wf}$).

$$h_{WF} = \frac{Nu.k_{WF}}{d_{it}} \tag{29}$$

$$Nu_{wf} = 3.657 + \frac{0.0677\left(Re_{h.wf}Pr_{wf}\frac{d_{it}}{L_t}\right)^{1.3}}{1 + 0.1Pr_{wf}\left(Re_{h.wf}\frac{d_{it}}{L_t}\right)^{0.3}} \text{ for } Re_{h.wf} < 2300 \tag{30}$$

$$Nu_{wf} = \frac{\frac{f}{8}\left(Re_{h.wf} - 1000\right)Pr_{wf}}{1 + 12.7\sqrt{\frac{f}{8}}\left({Pr_{wf}}^{0.67}\right)}\left(1 + \left(\frac{d_{it}}{L_t}\right)^{0.67}\right) \text{ for } 2300 < Re_{h.wf} < 10000 \tag{31}$$

$$Nu_{wf} = 0.047 {Re_{h.wf}}^{0.8} {Pr_{wf}}^{1/3} \text{ for } Re_{h.wf} > 10000 \tag{32}$$

Where k_{wf} is the thermal conductivity of the working fluid (kW/(m.K)), d_{it} is the tube inner diameter (m), f is the working fluid friction factor, L_t is tube length (m), and Pr_{wf} is the Prandtl number of the working fluid.

The overall convection coefficient in the shell and tube type heat exchanger (U), is formulated as Eq. (34), where the value is strongly influenced by the convection coefficient in the shell (h_{SW}) and tube (h_{WF}). Additionally, the thermal conductivity of the material also has a significant influence. The better the thermal conductivity of the material, the better the heat exchange that occurs.

$$U = \frac{1}{\frac{1}{h_{sw}} + \frac{t}{k_{pt}} + \frac{1}{h_{wf}} + R_f} \tag{33}$$

Where h_{sw} is the forced convection heat transfer coefficient of seawater (W/m^2K), h_{wf} is the convection heat transfer coefficient of the working fluid (W/m^2K), R_f is thermal resistance due to impurities ($m2K/W$), and k_{pt} is the thermal conductivity of the heat exchanger material (W/mK).

Fluid pressure drop is a key parameter that must be determined in calculating mass and heat equilibrium for the OTEC system. Pressure drop occurs in all fluids, both working fluid and seawater. The pressure drop in the working fluid is assumed to occur only in the heat exchanger. The calculation is divided into two parts: straight tubes and pass turns, with the pressure drop being the sum of the pressure drops across the tube and pass. The pressure drops in the straight tube and the pass turns are formulated in Eqs. (34) and 35.

$$\left(\Delta P_{WF}\right)_t = 4fN_t\frac{L_t {G_t}^2}{2d_{it}\rho_{wf}} \tag{34}$$

$$\left(\Delta P_{WF}\right)_p = 4N_t\frac{{G_t}^2}{2\rho_{wf}} \tag{35}$$

$$\Delta P_{WF} = \left(\Delta P_{WF}\right)_t + \left(\Delta P_{WF}\right)_p \tag{36}$$

Where G_t is the mass flow rate of the working fluid in each tube (kg/s) and ρ_{wf} is the density of the working fluid (kg/m^3).

In contrast, the pressure drop in seawater flow occurs in two components: the seawater pipe and the shell. In the shell, as with the working fluid pressure drop, the pressure drop is determined based on the mass flow rate of seawater after dividing the shell flow area (G_S). While in the pipe, the pressure drop is determined using the seawater flow velocity. The pressure drops in both components are formulated in Eq. (37) for the shell and Eq. (38) for the pipe.

$$(\Delta P_{Sw})_S = f\frac{l_S {G_S}^2}{2\rho D_s} \tag{37}$$

$$(\Delta P_{Sw})_P = f\frac{l_{WS}\rho {v_{sw}}^2}{2D} \tag{38}$$

Where G_s is the mass flow rate of seawater on the shell (kg/s), ρ_{wf} is the density of the working fluid (kg/m^3), l_S is shell length (m), l_{WS} is the length of the seawater pipe (m), and v_{sw} is the sea water flow speed in the pipe (m^3/s).

As stated in Eqs. (34), 37, and 38, the determination of fluid pressure drop is determined by the coefficient of friction factor of the fluid against the material (f). The determination of the friction coefficient factor in dynamic fluids can be done using the Darcy-Weisbach coefficient. In determining the coefficient of friction, the Reynolds number (Re) is the main parameter that determines the value of the coefficient of friction. The higher the Reynolds number of the flow, the higher the coefficient of friction against the pipe wall. The calculation of the friction coefficient of the working fluid and seawater is formulated in Eq. (39) [46].

$$\frac{1}{f} = \left(\frac{Re}{64}\right)^a \left(1.8log\frac{Re}{6.8}\right)^{2(1-a)b} \left(2log\frac{3.7D}{k}\right)^{2(1-a)(1-b)} \tag{39}$$

$$a = \frac{1}{1+\left(\frac{Re}{2720}\right)^9} \tag{40}$$

$$b = \frac{1}{1+\left(\frac{Re}{160\frac{D}{k}}\right)^2} \tag{41}$$

Where f is the Darcy-Weisbach friction coefficient, Re is the Reynolds number of fluid, k is the roughness of the pipe or shell material, and D is the diameter of the pipe or shell (m).

The net power output of the OTEC system ($\overline{W}$), is determined from the accumulated power generated by the generator (W_G), minus the power required to operate the working fluid pump ($W_{P,WF}$), surface seawater ($W_{P,WS}$), and deep seawater ($W_{P,CS}$). The power generated by the generator and required by the working fluid pump is determined by considering the enthalpy of each component in the cycle. The power requirement of the seawater pump is determined based on the pressure drop of seawater, as shown in Eqs. (42)–47.

$$\overline{W} = W_G - W_{P,WF} - W_{P,WS} - W_{P,CS} \tag{42}$$

$$W_G = m_{WF}(h_1 - h_2)\eta_T\eta_G \tag{43}$$

$$W_{P,WF} = m_{WF}(h_{4i} - h_3)/\eta_{P,WF} \tag{44}$$

$$W_{P,WS} = m_{WS}\Delta P_{WS}/\rho_{WS}\eta_{P,SW} \tag{45}$$

$$W_{P,CS} = m_{CS}\Delta P_{CS}/\rho_{CS}\eta_{P,SW} \tag{46}$$

$$\eta_S = \frac{\overline{W}}{Q_e} \tag{47}$$

Where m_{WF} is working fluid mass flow rate (kg/s), η_T is turbine efficiency, η_G is generator efficiency, $\eta_{P;WF,SW}$ is the pump efficiency of the working fluid and seawater, η_S is system efficiency (%), Q_e is the total heat exchange in the evaporator (kW), and $W_{P;WS,CS}$ is the decrease in surface and deep-sea water pressure (kPa).

4.1. Validation and benchmarking

Before system simulation, it is essential to conduct benchmarking to validate the simulation results against studies with similar topics. Benchmarking helps identify discrepancies between the desired and actual system performance or design, thereby enabling more effective refinement and improvement of the product or process under development. Simulations are carried out to determine the mass and heat balance of the cycle and to calculate the optimal net power output of the designed system.

The benchmarking process in this study is based on the findings presented by Bharathan [47], which aimed to assess the potential for increased economic benefits through effective seawater utilization and reduced maintenance costs. The OTEC systems discussed in the study utilize the Rankine cycle to generate electricity through the phase change of a working fluid, which drives a turbine connected to a generator. The Rankine cycle can be configured as a single, dual, or multi-stage process, with additional stages typically yielding higher power output. In [47], Ammonia was selected as the working fluid, as it yielded the highest net power output, albeit with safety concerns that require careful consideration.

Benchmarking was carried out using ASPEN + (version 11, AspenTech), which allows the construction and simulation of process models involving complex calculations. The software supports both modifying existing models and developing new ones. For this study, the benchmarking data consists of simulation results for single-cycle configurations. In addition to benchmarking, validation of the numerical methods and results was also conducted. Given that all equations used in the numerical simulations are formulated and parameterized based on system requirements, it is crucial to ensure the correctness of the selected equations. Therefore, validation was performed by comparing the numerical and analytical results with simulations from ASPEN+ and reference data. Unlike the benchmarking process, which involved both single and dual cycles, validation was limited to the single-cycle configuration, with the primary parameters outlined in Table 12. In the evaporator, a minimum temperature approach of 1.2 °C is applied between the hot and cold streams, while the condenser is modeled with a minimum approach of 1.0 °C. These values are specified in Aspen Plus as heat-transfer constraints to maintain both physical realism and numerical stability in the simulation, rather than representing superheating or subcooling of the working fluid. Accordingly, the working fluid exits the evaporator as saturated vapor and leaves the condenser as saturated liquid.

In addition to the main parameters outlined in Table 12, several supplementary parameters are applied specifically within each method. In the analytical approach, additional parameters are utilized for the single-cycle configuration, as detailed in Table 13. Meanwhile, the numerical method requires a broader set of input parameters, which are summarized in Table 14.

The simulation process is initiated by entering the type of working fluid, which in this case is water (H_2O) and ammonia, and then checking the fluid properties. Subsequently, the Base Method was selected for calculating the physical properties of the components within the simulation. The Base Method provides mathematical models and parameters for estimating properties such as enthalpy, entropy, vapor pressure, and density. In OTEC systems, a suitable thermodynamic method is the Peng-Robinson (PR) equation of state, which is capable of assessing the

Table 12
Main input parameters for validation and benchmarking of numerical and analytical methods.

Parameter	Value
Surface sea water temperature (°C)	26
Mass flow rate of surface seawater (kg/s)	50,000
Deep-sea water temperature (°C)	4.5
Mass flow rate of deep-sea water (kg/s)	28,450
Working fluid and seawater pump efficiency (%)	0.72
Minimum temperature on the evaporator (°C)	1.2
Minimum temperature of the condenser (°C)	1.0
Working fluid	Ammonia

Table 13
Cycle input parameters.

Parameter	Value
Surface sea water pressure (bar)	1
Deep-sea water pressure (bar)	1
Working fluid temperature 1 (°C)	11.72
Working fluid pressure 1 (bar)	6.47
Working fluid mass flow rate 1 (kg/s)	580

Table 14
Numerical method benchmarking calculation parameters.

Parameter	Value
Generator efficiency (%)	0.94
Turbine efficiency (%)	0.75
Heat exchanger thermal conductivity (kW/m^{2}K)	4.693
Total heat transfer area on the evaporator (m^2)	41,500
Total heat transfer area of the condenser (m^2)	42,500
Working fluid mass flow rate (kg/s)	580
Sea water flow speed (m/s)	1.5
Sea water pipe diameter (m)	1
Length of surface seawater pipe (m)	100
Length of deep-sea water pipe (m)	2800

thermophysical behavior of complex fluid mixtures, including phase changes. This method considers molecular interactions, pressure, and temperature effects, thereby ensuring the accuracy of the simulation results [48].

After defining the fluid parameters, the simulation proceeds to the next stage by constructing the Rankine cycle circuit, as illustrated in Fig. 5. The circuit consists of standard components typically found in a Rankine cycle, including pumps, heat exchangers, and turbines.

In this cycle, streamlines are assembled to facilitate mass equilibrium calculations. The system is considered balanced when the key properties—such as temperature, pressure, specific volume, and phase—of the input stream match those of the output. Once the circuit is constructed, the parameters for the working fluid, warm seawater input, and cold seawater input are defined. Adjustments are then made to the pump, evaporator, condenser, and turbine to ensure that the output conditions align with the initial design specifications.

The working fluid pump increases the pressure by 2.49 bar with an efficiency of 0.58, ensuring that the working fluid reaches the required operating pressure for stable evaporation under saturated conditions in the evaporator. Meanwhile, the seawater pump operates with an efficiency of 0.72, providing pressure increases of 0.72 bar and 0.3 bar for the condenser and evaporator circuits, respectively. These pressure rises are not only intended to circulate fluids through the heat exchangers but also to compensate for the pressure drops that occur along the piping and heat exchanger passages, thereby maintaining hydraulic stability and the overall energy balance of the cycle. The turbine has an efficiency of 0.75 and operates with a pressure ratio of 0.722. Once all settings are configured, the simulation is executed.

The simulation results show that the working fluid absorbs 175,784,039 cal/*sec* (735,972.61 kW) of heat in the evaporator, transitions into a superheated vapor, and passes through the turbine, where it reduces its temperature and pressure while increasing its volumetric flow rate. In the condenser, although the temperature does not change significantly, the phase transition from vapor to liquid requires 171,492,691 cal/*sec* (718,005.59 kW) of heat removal. The turbine generates −18,377 kW of power, while the working fluid, warm water, and cold-water pumps consume 400, 2098, and 2807 kW of power, respectively. These results, along with the flow conditions, are illustrated in Fig. 6.

The comparison of the simulation results with previous research is presented in Fig. 6, where Fig. 6(a) corresponds to the simulation results from the earlier study. In contrast, Fig. 6(b) depicts the results obtained in the present work. The comparison reveals a remarkable agreement, indicating that the patterns of heat transfer, phase transitions of the working fluid, and trends in power output observed in this study are strongly consistent with the findings reported previously. Table 15 presents a comparison between the simulation results from the previous study and those obtained in the present work, focusing on the generator power output and the system's parasitic power. During the last study,

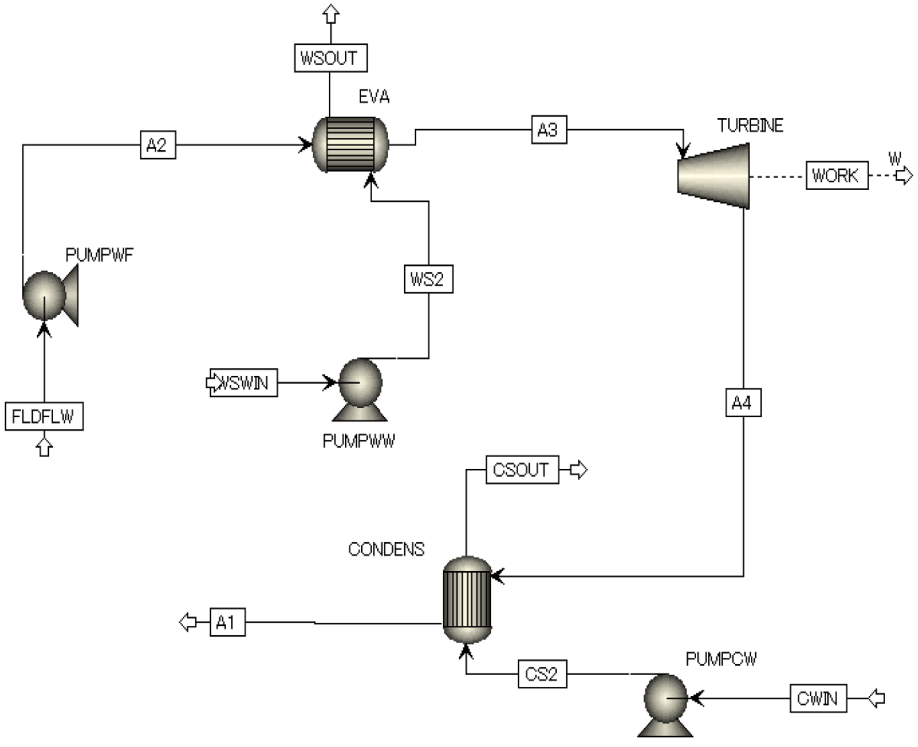

Fig. 5. Rankine cycle circuit schematic in ASPEN+ software.

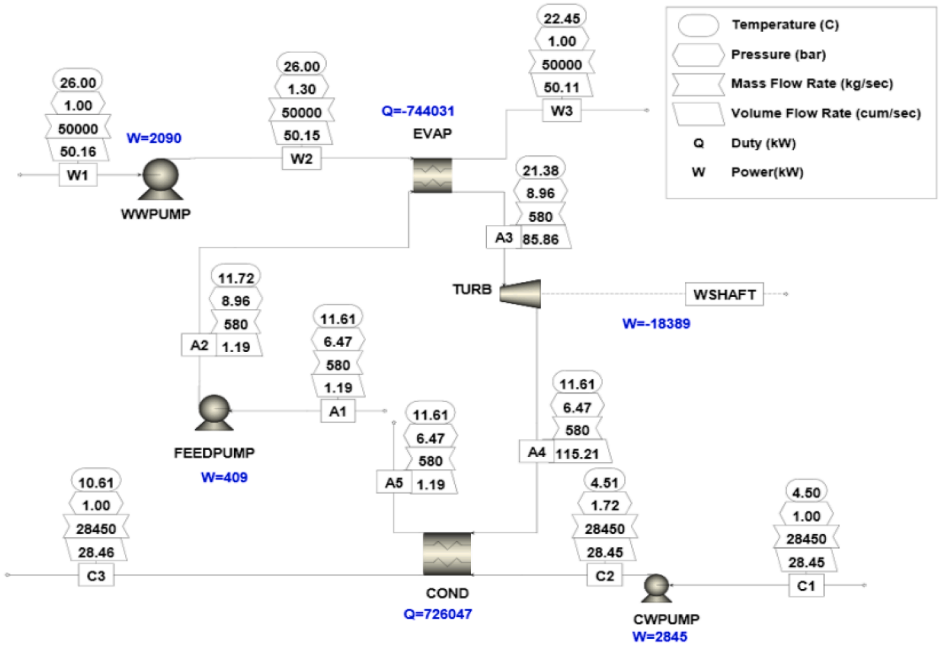

Fig. 6. Single cycle simulation results (a) benchmarking [47], and (b) present simulation.

Table 15
Comparison of simulation results with single-cycle journals.

Parameters	Journal [47]	Numerical (ASPEN +)	Errors
Power Output	18,389 Kw	18,377 kW	0.065 %
Parasitic Power	5344 kW	5296 kW	0.89 %

the power output was reported as 18,389 kW, while the current simulation produced 18,377 kW, corresponding to an error of only 0.065 %. For the parasitic power, the previous result was 5344 kW, whereas the present simulation yielded 5296 kW, with an error of just 0.89 %. Both the power output and parasitic power show errors of <1 %, confirming that the benchmarking simulation is valid.

After the numerical method using ASPEN+ software was validated, the validation results from ASPEN+ were compared with those from the analytical method (in-house code written in MATLAB), which will be

Table 16
Comparison of simulation results between numerical and analytical methods.

Parameters	Numerical (ASPEN +)	Analytical (In-house Code)	Errors
Power Output	18,377 kW	18,367 kW	0.05 %
Parasitic Power	5296 kW	5590.5 kW	5.3 %

used for the overall calculation. The analytical method follows the flowchart in Fig. 1 and the calculation process already described in subSection 4.1. As shown in Table 16, the difference in power output is only 10 kW, or about 0.05 %. The larger difference is found in the parasitic power requirement, where the discrepancy between the two methods reaches 294.5 kW, or >5 %. Nevertheless, this difference is still within a normal range, and therefore, both approaches can be used consistently to determine the performance of the OTEC system.

4.2. Power generation analysis results

4.2.1. Power generation performance

The calculations and simulations are evaluated based on several parameters, including the power requirement of the working fluid pump, the working fluid temperature after the evaporator (T_1), the working fluid pressure after the evaporator (P_1), the working fluid temperature after the condenser (T_3), the working fluid pressure after the condenser (P_3) and the power generated by the turbine. The simulation is performed by targeting the values of T_1, P_1, T_3 and P_3 to match those obtained from the calculations. T_3 and P_3 are input parameters to provide the initial temperature and pressure of the working fluid, along with the mass flow rate of the working fluid. Once the simulation is executed, the results include the turbine power output. The power consumed by the working fluid pump is a critical factor, as it significantly influences T_1 and P_1, which in turn affect the turbine's power output.

Each working fluid has different thermophysical properties; therefore, system parameters must be adjusted to ensure mass balance. Additionally, the efficiencies of the pump and turbine are calibrated to realistic values, reflecting plausible operating conditions. The input parameters used for each working fluid are listed in Table 17.

Based on the power output and working fluid pump power data within the cycle, it is observed that the power output values across different working fluids do not differ significantly. As presented in Table 18, for example, ammonia produces a power output of 131.278 kW with a pump power requirement of 2.972 kW, while R-32 yields a slightly higher output of 139.70 kW with a pump power requirement of 11.96 kW. Based on the power output and working fluid pump power data within the cycle, it is observed that the power output values across different working fluids do not differ significantly. As shown in Table 18, R32 achieves the highest gross power of 139.70 kW, but also requires the highest pump power of 11.96 kW, resulting in a net output comparable to that of other fluids. Ammonia, on the other hand, produces 131.28 kW with only 2.97 kW of pump power. This advantage arises from its relatively low suction pressure at the pump inlet (P1 ≈ 9.2 bar), which reduces the compression ratio, combined with a relatively small working fluid mass flow rate (7 kg/s). Both factors minimize the required pumping work. In contrast, R134a requires the highest mass flow rate (44.5 kg/s) and approximately 6.24 kW of pump power, while R32 operates at a higher P1 (~15.7 bar) with a mass flow rate of 27.8 kg/s, which explains its higher pump consumption. In summary, variations in pump work among the fluids are directly governed by differences in suction pressure and mass flow, with ammonia achieving the most favorable balance between net power output, pumping cost, and mass flow demand.

Table 17
Analytical method input parameter.

Parameters	Working fluid			
	Ammonia	R22	R32	R134a
Evaporator area (m^2)	1029.2	2376.9	1249.7	2940.5
Condenser area (m^2)	1029.2	2376.9	1249.7	2940.5
Evaporator U value (kW/m^2)	2489.9	2363.6	2556.8	2395.2
Condenser U value (kW/m^2)	2203.7	2218.2	2283.8	2258.4
Mass flow rate of working fluid (kg/s)	7	43	27.8	44.5
Mass flow rate of surface seawater (kg/s)	415	425	410	430
Mass flow rate of deep-sea water (kg/s)	390	405	390	410
T_1 (°C)	22.42	22.2	21.92	21.83
P_1 (bar)	9.17	9.6	15.67	6.03
T_3 (°C)	14.74	14.55	13.77	14.06
P_3 (bar)	7.21	7.73	12.57	4.81
Working fluid pump power (kW)	2.97	8.7	11.9	6.24
Surface sea water pump power (kW)	0.247	0.266	0.238	0.275
Deep-sea water pump power (kW)	4.170	4.669	4.170	4.844

Table 18
Working fluid simulation results.

Results	Ammonia	R-22	R-32	R-134
Power output (kW)	131.278	134.309	139.70	133.252
Working fluid pump power (kW)	2.972	8.79	11.96	6.239

4.2.2. Main component specification

Although they have the exact basic component specifications, each working fluid requires different component specifications to achieve the target power output capacity of 120 kW. The performance of the working fluid in OTEC systems can be observed from its component requirements. The larger the system components required, the lower the performance of the working fluid in the OTEC system. Given that the main specifications of the seawater pipes are uniform across all systems, variations emerge in the required seawater mass flow rates. As presented in Table 19, the mass flow rates of deep and surface seawater differ. This is influenced by the pressure loss experienced by seawater as it travels through the deep seawater pipe. Due to the greater pipe length, the pressure drop in the deep seawater pipeline is significantly higher, even when the mass flow rate remains constant.

Furthermore, as shown in Table 19, R134a requires the highest total seawater mass flow rate (430 for surface seawater and 410 for deep seawater), followed by R22, ammonia, and R32. With the pipe diameter kept constant, variations in mass flow rate directly affect the flow velocity of seawater. In this context, the relationship between mass flow rate and flow velocity is linear; higher mass flow rates lead to higher flow velocities. However, the actual flow velocities of seawater through the pipes remain relatively low, at approximately 5×10^{-3} m/s across all working fluids (see Table 20). This indicates that the current pipe dimensions are oversized and have not been fully utilized. Consequently, either the pipe size could be reduced or the system could be scaled up to accommodate a higher power output.

A significant distinction between systems using different working fluids lies in the heat exchanger size requirement. As defined in Eqs. (2) and 5, to achieve a total heat transfer sufficient to produce 120 kW of power, each system must attain the same overall heat transfer coefficient-area product (UA value). However, due to varying thermophysical properties—particularly thermal conductivity—each working fluid demands a different number of heat exchanger tubes to meet the required UA.

As shown in Table 21, the number of tubes required differs significantly across the systems, depending on the working fluid. For ammonia and R32, the requirements are relatively close, with ammonia requiring approximately 4200 tubes for both the condenser and evaporator, while

Table 19
Requirements for the mass flow rate of seawater in each system with different working fluids.

Working Fluid	Sea Water Mass Flow Rate (kg/s)	
	Surface	Deep
Ammonia	415	390
R32	410	390
R22	425	405
R134a	430	410

Table 20
Seawater flow speed requirements in each system with different working fluids.

Working fluid	Velocity × 10^{-3} (m/s)	
	Surface	Deep
Ammonia	5.2	4.8
R32	5.1	4.8
R22	5.3	5.0
R134a	5.4	5.1

Table 21
The required number of tubes is between each system, which uses different working fluids.

Working fluid	Number of tubes	
	Evaporator	Condenser
Ammonia	4200	4200
R32	5100	5100
R22	9700	9700
R134a	12,000	12,000

R32 requires about 5100 tubes. The difference between these two systems is therefore only about 1100 tubes. In contrast, the systems using R22 and R134a require a significantly larger number of tubes, with approximately 9700 and 12,000 tubes, respectively, indicating a considerably higher design demand.

Under the required number of tubes, the shell diameter of the heat exchanger increases proportionally. As presented in Table 22, systems utilizing ammonia and R32 as working fluids require shell diameters of <1 m In contrast, systems employing R22 and R134a exhibit shell diameter requirements exceeding 1 m This outcome highlights the influence of working fluid properties on the dimensional configuration of the heat exchanger, particularly in terms of space and material efficiency considerations.

In calculating the power production capacity of the generator in the OTEC system, the mass flow rate of the working fluid becomes a key factor in the calculation. Thus, as the target capacity is 120 kW, the mass flow rate of the working fluid used in the future should be able to reach or approach the net power output of 120 kW. However, the addition of the working fluid flow rate is linear with the increase in the overall convection coefficient of the heat exchanger (U). In reality, increasing the mass flow rate of the working fluid does not necessarily increase the generation and net power output of the OTEC system. As shown in Figs. 7–10, the relentless increase of working fluid causes a bell-shaped graph of power versus working fluid. In each system with different working fluids, it is necessary to consider the mass flow rate corresponding to the highest power generation or the point at the top of the graph.

Furthermore, the range of working fluid mass flow rates exhibits a considerable difference between each system. The system utilising an ammonia working fluid displays the lowest mass flow rate range among systems employing other working fluids. Conversely, systems employing R22 and R134a working fluids exhibit a range of working fluid mass flow rates that tend to be similar in magnitude. As shown in Fig. 7,8,9, Fig. 10, the relentless increase of working fluid causes a bell-shaped graph of power versus working fluid. In each system with different working fluids, it is necessary to consider the mass flow rate corresponding to the highest power generation or the point at the top of the graph. Furthermore, the range of working fluid mass flow rates exhibits a considerable difference between each system. The system utilising an ammonia working fluid displays the lowest mass flow rate range among systems employing other working fluids. Conversely, systems employing R22 and R134a working fluids exhibit a range of working fluid mass flow rates that tend to be similar in magnitude.

Table 22
Shell diameter requirements between systems with different working fluids.

Working fluid	Shell diameter (m)	
	Evaporator	Condenser
Ammonia	0.83	0.83
R32	0.90	0.90
R22	1.16	1.16
R134a	1.26	1.26

The bell-shaped relationship between power and flow rate is explained by two main factors: at higher flow rates, pressure losses in the heat exchangers increase. In contrast, the temperature driving force for heat transfer becomes less effective. These effects counteract the potential thermal gain, resulting in a peak point that marks the balance between the added pumping work and the heat transfer benefits. The optimal flow rate for each working fluid was identified by systematically varying the mass flow rate while keeping other parameters constant, and selecting the maximum net output observed.

Based on the power versus mass flow rate graph, the optimal mass flow rate for each working fluid system has been identified. The corresponding values for the four systems using different working fluids are presented in Table 23. Consistent with the observed differences in mass flow rate ranges, the optimal mass flow rate for each working fluid also varies significantly. The system utilizing ammonia demonstrates the lowest optimal mass flow rate at 7 kg/s, while R134a and R22 exhibit the highest values at 44.5 kg/s and 43 kg/s, respectively.

For further discussion, a sensitivity analysis was conducted by varying the component efficiencies by ±5 %, using the reference values presented in Table 9. Additionally, the surface and deep seawater temperatures were varied by ±1 °C. In this analysis, the efficiencies of the four components were assumed as a single package, and the same approach was applied to the seawater temperatures. Cross variations were then performed, resulting in nine possible outcomes for each working fluid, as presented in Table 24.

The results indicate that when the efficiencies of all components are reduced by 5 %, the target power output cannot be achieved, with the net output averaging only around 100 kW for each working fluid. Conversely, increasing the component efficiencies by 5 % leads to an additional net power output of approximately 24–27 kW. Meanwhile, the variation of surface and deep seawater temperatures by ±1 °C shows no significant effect, with a difference of only about 1 kW in net output.

4.3. Optimization process

The results of the calculations and analysis were obtained after identifying the most optimal OTEC system using four selected working fluids. These fluids are ammonia, R32, R22, and R134a, which were re-evaluated to determine the most suitable working fluid. The selection was based on the overall performance of each fluid within the OTEC system.

4.3.1. Power generation parameters

As in the initial assessment of the ten working fluids, the enthalpy evaluation of the four selected working fluids — namely, ammonia, R32, R22, and R134a — is conducted using the same criteria. The assessment uses a scale ranging from 1 to 5, with ammonia receiving the highest score, while R134a and R22 obtain the lowest score of 1. The range of values for each parameter is presented in Table 25.

The flow rate of the working fluid is a primary determinant of the system's power generation capacity. A lower working fluid flow rate tends to enhance heat exchange efficiency. However, it also influences the power requirement of the working fluid pump, although this effect is not always dominant. The working fluid flow rate is assessed on a maximum scale of 4, based on the established criteria. A lower seawater flow rate can reduce the operational load on the seawater pumps and consequently decrease the overall power requirement. The characteristics of each working fluid, particularly its thermal conductivity,

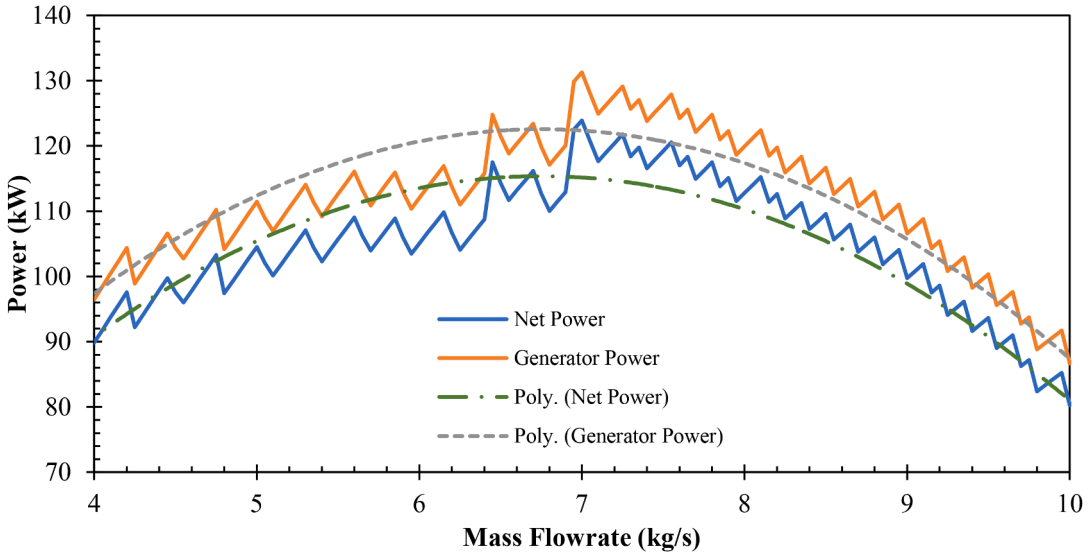

Fig. 7. Results of power generation in a system with ammonia working fluid.

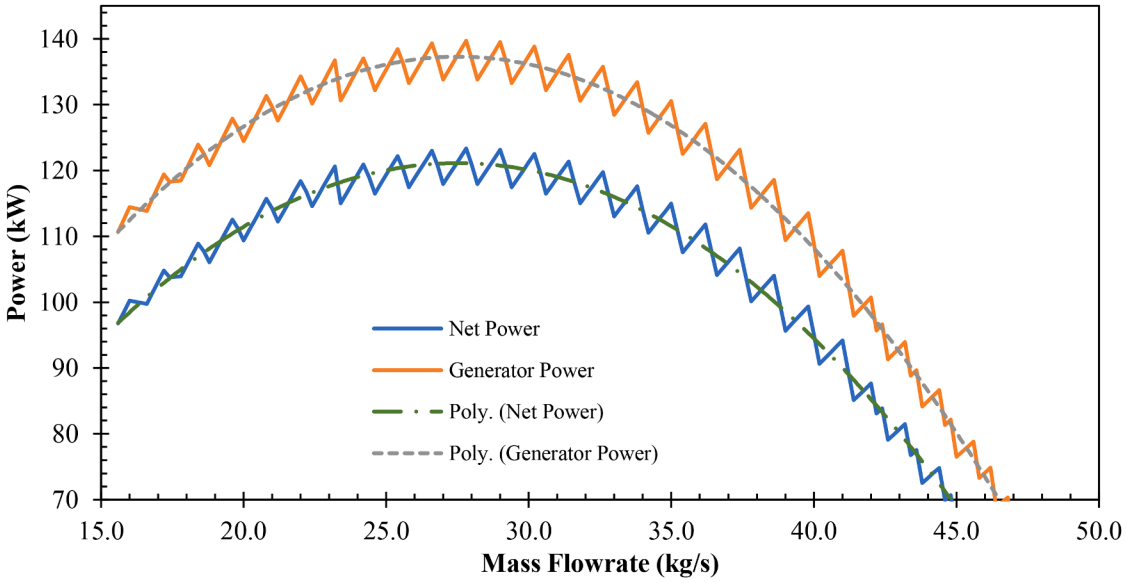

Fig. 8. Results of power generation in a system with R32 working fluid.

significantly influence the required mass flow rate of seawater. The assessment of seawater flow rate is based on the deep seawater mass flow rate, which serves as a standard reference for comparison.

The heat exchanger assessment considers two primary factors: the number of tubes and the shell diameter. Since the shell diameter is directly and linearly related to the number of tubes, the evaluation focuses mainly on the number of tubes required for each working fluid system. The total pump power requirement, also known as parasitic power, plays a crucial role in selecting the optimal working fluid, as it significantly affects the system's operational load. For this analysis, all working fluids are assumed to generate the same annual electricity output based on a fixed capacity target of 120 kW. Although the differences in electricity output are not substantial, the annual electricity production remains a key parameter in the overall evaluation of working fluid performance.

4.3.2. Safety, environmental, and cost parameters

In addition to evaluating the efficiency of each working fluid in power generation, it is also essential to consider the safety of the system and its environmental impact. These aspects are critical to ensure the feasibility and sustainability of OTEC operations. Therefore, safety and environmental parameters are integrated into the overall assessment. For the flammability parameter, a maximum score of 4 is used. In this category, only ammonia receives a score of 2 due to its higher flammability risk, while R134a and R22 each receive the maximum score of 4, indicating non-flammable characteristics. In terms of toxicity, ammonia again gets a lower score of 2, whereas R32, R22, and R134a are each assigned a score of 4, reflecting a higher level of safety for handling and use.

Regarding environmental impact, the Global Warming Potential (GWP) of each working fluid is considered, as listed in Table 6. A higher GWP value represents a greater risk if the fluid leaks into the environment. Based on the GWP evaluation, R134a and R22 are assigned the lowest score of 1 due to their significant environmental impact. Meanwhile, R32 receives a score of 3, and ammonia achieves a score of 5, indicating minimal global warming potential. The cost parameter is assessed using a maximum score of 5. Working fluids with a market cost below $1000 are given the highest score of 5, while those exceeding this

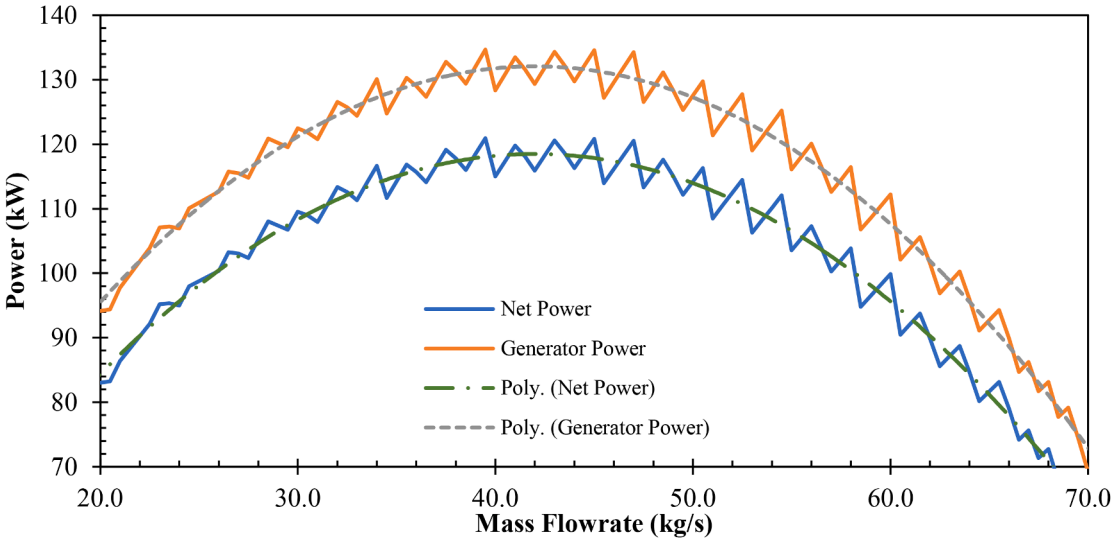

Fig. 9. Results of power generation in a system with R22 working fluid.

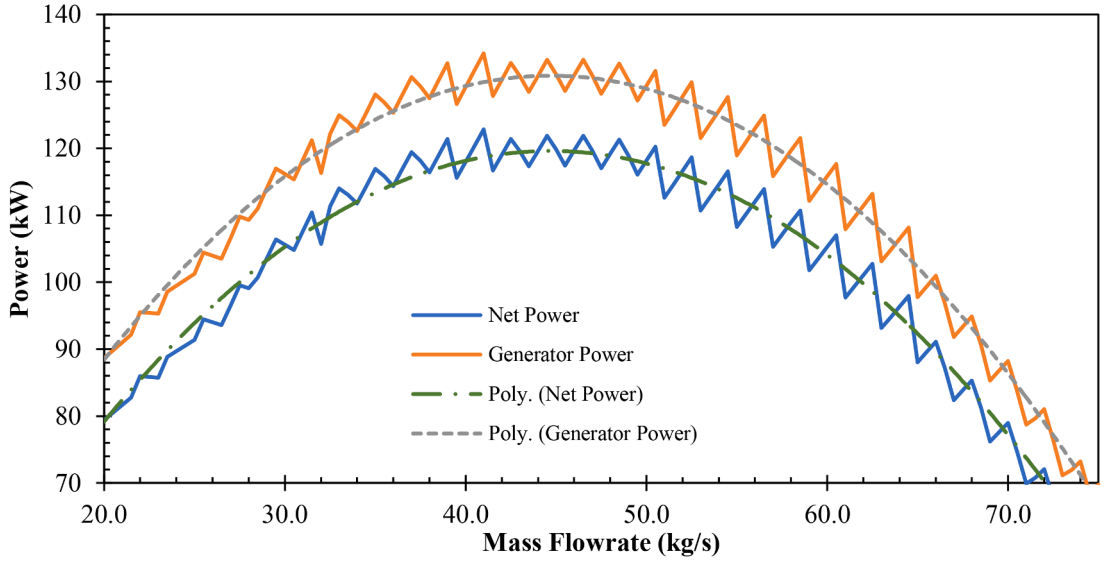

Fig. 10. Results of power generation in a system with R134a working fluid.

Table 23
Best mass flow rate for each working fluid.

Working fluid	Mass flow rate of working fluid (kg/s)
Ammonia	7
R32	27.8
R22	43
R134a	44.5

cost threshold are assigned a score of 4. According to this assessment, ammonia is rated 5, while R32, R22, and R134a each receive a score of 4.

4.3.3. *Optimization results*

The results of the assessment, covering all parameters including the performance and characteristics of the four working fluids, are presented in Table 26. Ammonia and R32 achieved the highest total scores compared to R22 and R134a. Ammonia leads with a total score of 37, maintaining a significant margin of 9 points above R32 in second place. This high score is primarily attributed to ammonia's superior

Table 24
Sensitivity analysis.

Working Fluid	Component efficiencies	Net Power Output (kW)		
		Temperature −1 °C	Temperature +0 °C	Temperature +1 °C
Ammonia	−5 %	99.357	100.773	100.291
	+0 %	121.240	122.977	122.424
	+5 %	145.725	147.821	147.187
R32	−5 %	99.464	98.506	98.603
	+0 %	123.874	122.817	123.065
	+5 %	151.045	149.871	150.280
R22	−5 %	98.492	98.676	98.410
	+0 %	121.829	121.073	122.077
	+5 %	147.996	147.159	148.447
R134a	−5 %	100.267	99.913	99.977
	+0 %	123.599	123.098	123.112
	+5 %	149.634	148.974	148.934

Table 25
Range of values for the parameters.

Point	Working fluid flow rate (kg/s)	Seawater flow rate (kg/s)	Number of heat exchanger tubes	Pump power requirements (kW)	Annual electrical energy production (MWh)
4	1 – 10	300 – 350	2500 – 5000	1 – 5	30 – 50
3	10 – 20	350 – 400	5000 – 7500	5 – 10	20 – 30
2	20 – 30	400 – 450	7500 – 10,000	10 – 15	10 – 20
1	30 – 50	450 – 500	10,000 – 15,000	15 – 20	1 – 20

Table 26
Results of the assessment of the four working fluids.

Parameters	Ammonia	R32	R22	R134a
Enthalpy	5	2	1	1
Working fluid flow rate	4	2	1	1
Sea water flow rate	3	3	2	2
Heat exchanger	4	3	2	1
Parasitic power	3	1	2	2
Annual energy production	4	3	2	1
Flammability	2	3	4	4
Toxicity	2	4	4	4
GWP	5	3	1	1
Cost	5	4	4	4
TOTAL	**37**	**28**	**23**	**21**

performance across nearly all evaluated parameters. In contrast, the performance scores of R22 and R134a remain relatively low, mostly ranging between 1 and 2. These results indicate that ammonia and R32 not only demonstrate better thermodynamic performance but also require more efficient system components, making them more favourable for OTEC system applications under the specified design assumptions.

To ensure the robustness of the results, a sensitivity analysis was performed with ±10 % adjustments in the weighting factors. In this test, parameters with a maximum score of 5 were reduced by 10 % of their values, while those with a maximum score of 4 were increased by 10 %. The results, as shown in Table 27, indicate that the optimization still yields the same ranking of working fluids: Ammonia, R32, R22, and R134a. This consistency occurs because Ammonia also demonstrates superior values in the parameters with a maximum score of 4, thereby maintaining its leading position in the overall ranking.

5. Conclusions

OTEC power plants represent a type of marine renewable energy that generates electricity indirectly from solar energy by utilizing the temperature difference between warm surface seawater and cold deep seawater. This study addressed the challenges of selecting a working fluid and designing a preliminary cold-water pipeline, both of which significantly influence energy conversion in closed-cycle systems. Importantly, the study contributes by integrating multi-criteria screening with validated cycle modeling, explicitly linking component-level implications—such as tube counts, shell diameters, and seawater flow requirements—to the choice of working fluids for OTEC systems. This novelty highlights how fluid selection translates into practical design consequences and ultimately determines the achievable net power output.

The selection of the working fluid was conducted in two stages. The initial screening included ten candidate fluids: ammonia, R152a, R134a, R32, R22, R1270, R600a, R290, R744, and R245fa. Selection criteria included generation characteristics, safety (in terms of flammability and toxicity), and cost. Four fluids with the highest scores—ammonia, R134a, R32, and R22—advanced to the detailed cycle analysis stage.

Table 27
Results of the sensitivity test of the four working fluids.

Parameters	Ammonia	R32	R22	R134a
Enthalpy	4.5	1.8	0.9	0.9
Working fluid flow rate	4.4	2.2	1.1	1.1
Sea water flow rate	3.3	3.3	2.2	2.2
Heat exchanger	4.4	3.3	2.2	1.1
Parasitic power	3.3	1.1	2.2	2.2
Annual energy production	4.4	3.3	2.2	1.1
Flammability	2.2	3.3	4.4	4.4
Toxicity	2.2	4.4	4.4	4.4
GWP	4.5	2.7	0.9	0.9
Cost	4.5	3.6	3.6	3.6
TOTAL	**37.7**	**29**	**24.1**	**21.9**

In the second stage, the influence of these fluids on leading equipment (heat exchanger and working fluid pump) and generation performance (capacity factor, efficiency, annual electricity) was evaluated. Ammonia achieved the highest overall score due to its very high latent heat (1169.95 kJ/kg) and low cost, consistent with previous studies [26, 29]. Its toxicity (NFPA health rating 3) lowers its safety score, but its thermodynamic advantage outweighs this. R32 delivered slightly higher gross power (139.7 kW) but required higher suction pressure (P_1 = 15.67 bar) and pump work, which reduced its net output and penalized its total score. R22 (P_1 = 9.6 bar) and R134a showed lower efficiency, lower enthalpy (R22: 183.73 kJ/kg; R134a: 178.7 kJ/kg), larger heat exchangers, and higher GWP (R22: 1760; R134a: 1300), which explains their lower ranks. R32 outperforms R22/R134a by balancing moderate enthalpy (272.93 kJ/kg) with mid-range GWP (677), offering a pragmatic compromise between performance and environmental impact. It should be noted that the use of R22 and R134a, both with high GWP, requires particular attention due to their ecological impacts; in this study they are included only for comparison, given regulatory concerns over their high GWP and non-zero ODP.

This study assumes fixed ambient conditions (26 °C/4.5 °C) and constant system efficiencies. Seasonal ocean temperature variations, fouling, or other operational effects were not considered. Future work could investigate how fluid rankings change in response to variations in ocean temperature or different scale-up targets. Additionally, only pure single-component fluids were considered. Prior work suggests ammonia–water mixtures may further improve OTEC performance; future studies could extend the framework to explore novel low-GWP refrigerants (e.g., R1234ze) and assess their potential performance and environmental advantages in OTEC systems. While the current analysis is deterministic, the robustness of the rankings to small parameter changes could be explored; given ammonia's considerable enthalpy advantage, its top ranking is expected to be robust.

Choosing ammonia can significantly reduce equipment size (heat exchanger and pumps), potentially lowering capital costs despite stricter safety requirements. R32 may be considered if ammonia use is restricted, though its higher pumping cost offsets part of its higher thermal output.

CRediT authorship contribution statement

Ristiyanto Adiputra: Writing – review & editing, Writing – original draft, Methodology, Investigation, Formal analysis, Data curation, Conceptualization. **Rasgianti:** Supervision, Software, Methodology, Funding acquisition, Conceptualization. **Ariyana Dwiputra Nugraha:** Writing – review & editing, Supervision, Methodology, Funding acquisition, Conceptualization. **Navik Puryantini:** Supervision, Software, Project administration, Methodology, Conceptualization. **Gerry Giliant Salamena:** Resources, Project administration, Investigation, Data curation. **Aditya Rio Prabowo:** Writing – review & editing, Supervision,

Software, Methodology, Funding acquisition, Conceptualization.

Declaration of competing interest

The authors declare that they have no known competing financial interests or personal relationships that could have appeared to influence the work reported in this paper.

Acknowledgement

This research was made possible by the financial assistances from the Ocean Research for Blue Economy research program administered by BRIN's Research Organization for Earth Sciences and Maritime under a project entitled "Comprehensive oceanographic studies on internal tides in supporting the potential of Ocean Thermal Energy Conversion: A case study in Ambon Bay, Maluku" (Grant number: 2/III.4/HK/2025).

Data availability

The authors confirm that the data supporting the findings of this study are available within the article.

References

[1] Rasgianti, R. Adiputra, R.B. Sitanggang, N. Puryantini, N. Firdaus, Ocean thermal energy conversions (OTEC) working fluid comparison based on the numerical and analytical analysis, in: 2024 International Conference on Technology and Policy in Energy and Electric Power, IEEE, 2024, pp. 222–227, https://doi.org/10.1109/ICT-PEP63827.2024.10733395.

[2] Z.U. Islam, M.S. Hossain Lipu, S.T. Meraj, A.M. Fuad, T. Rahman, M.A. Islam, M.R. Sarker, Hybrid renewable energy systems towards sustainable development in Bangladesh: configurations, optimizations, applications, challenges and future pathways, results eng. 27 (2025) 105728. https://doi.org/10.1016/j.rineng.2025.105728.

[3] Rasgianti, R. Adiputra, A.D. Nugraha, R.B. Sitanggang, W.W. Pandoe, Aprijanto, T. Yasunaga, M.A. Santosa, System parameters sensitivity analysis of ocean thermal energy conversion, Emerg. Sci. J. 8 (2024) 428–448, https://doi.org/10.28991/ESJ-2024-08-02-04.

[4] R. Adiputra, T. Utsunomiya, Stability based approach to design cold-water pipe (CWP) for ocean thermal energy conversion (OTEC), Appl. Ocean Res. 92 (2019) 101921, https://doi.org/10.1016/j.apor.2019.101921.

[5] J.H. VanZwieten, L.T. Rauchenstein, L. Lee, An assessment of Florida's ocean thermal energy conversion (OTEC) resource, Renew. Sustain. Energy Rev. 75 (2017) 683–691, https://doi.org/10.1016/j.rser.2016.11.043.

[6] M. Shalby, A. Marachli, A.A. Salah, Working fluid selection and performance analysis for subcritical organic rankine cycles, Results. Eng. 25 (2025) 104120, https://doi.org/10.1016/j.rineng.2025.104120.

[7] M.-H. Yang, R.-H. Yeh, Analysis of optimization in an OTEC plant using organic Rankine cycle, Renew. Energy 68 (2014) 25–34, https://doi.org/10.1016/j.renene.2014.01.029.

[8] N. Abas, A.R. Kalair, N. Khan, A. Haider, Z. Saleem, M.S. Saleem, Natural and synthetic refrigerants, global warming: a review, Renew. Sustain. Energy Rev. 90 (2018) 557–569, https://doi.org/10.1016/j.rser.2018.03.099.

[9] T.H. Nakib, M. Hasanuzzaman, N.A. Rahim, M.A. Habib, N.N. Adzman, N. Amin, Global challenges of ocean thermal energy conversion and its prospects: a review, J. Ocean. Eng. Mar. Energy 11 (2025) 197–231, https://doi.org/10.1007/s40722-024-00368-4.

[10] M.I. Habib, R. Adiputra, A.R. Prabowo, E. Erwandi, N. Muhayat, T. Yasunaga, S. Ehlers, M. Braun, Internal flow effects in OTEC cold water pipe: finite element modelling in frequency and time domain approaches, Ocean Eng. 288 (2023) 116056, https://doi.org/10.1016/j.oceaneng.2023.116056.

[11] R. Adiputra, T. Utsunomiya, Finite element modelling of ocean thermal energy conversion (OTEC) cold water pipe (CWP), in: International Conference on Offshore Mechanics and Arctic Engineering, 2022. V004T05A012.

[12] A.M. Naufal, A.R. Prabowo, T. Muttaqie, A. Hidayat, R. Adiputra, N. Muhayat, S. Hadi, I. Yaningsih, Three-point bending assessment of cold water pipe (CWP) sandwich material for ocean thermal energy conversion (OTEC), Procedia Struct. Integr. 47 (2023) 133–141, https://doi.org/10.1016/j.prostr.2023.07.004.

[13] P.W. Adie, A.R. Prabowo, T. Muttaqie, R. Adiputra, N. Muhayat, H. Carvalho, N. Huda, Non-linear assessment of cold water pipe (CWP) on the ocean thermal energy conversion (OTEC) installation under bending load, Procedia Struct. Integr. 47 (2023) 142–149, https://doi.org/10.1016/j.prostr.2023.07.005.

[14] P.W. Adie, R. Adiputra, A.R. Prabowo, E. Erwandi, T. Muttaqie, N. Muhayat, N. Huda, Assessment of the OTEC cold water pipe design under bending loading: a benchmarking and parametric study using finite element approach, J. Mech. Behav. Mater. 32 (2023), https://doi.org/10.1515/jmbm-2022-0298.

[15] R. Adiputra, T. Utsunomiya, Design optimization of floating structure for a 100 MW-net ocean thermal energy conversion (OTEC) power plant, Ocean Renew, Energy Am. Soc. Mech. Eng. 10 (2018), https://doi.org/10.1115/OMAE2018-77539.

[16] F. Sinama, M. Martins, A. Journoud, O. Marc, F. Lucas, Thermodynamic analysis and optimization of a 10 MW OTEC Rankine cycle in Reunion Island with the equivalent gibbs system method and generic optimization program GenOpt, Appl. Ocean Res. 53 (2015) 54–66, https://doi.org/10.1016/j.apor.2015.07.006.

[17] M.A.S.S. Ravagnani, A.P. Silva, E.C. Biscaia, J.A. Caballero, Optimal design of shell-and-tube heat exchangers using particle swarm optimization, Ind. Eng. Chem. Res. 48 (2009) 2927–2935, https://doi.org/10.1021/ie800728n.

[18] K.S. et al. K. Silaipillayarputhur, et al., The design of shell and tube heat exchangers - A review Int. J. Mech. Prod. Eng. Res. Dev. 9 (2019) 87–102, https://doi.org/10.24247/ijmperdfeb201910.

[19] Y. Mochida, S. Kawano, T. Takahata, M. Miyoshi, Performance of the heat exchangers of a 100-kW (Gross) OTEC plant, J. Sol. Energy Eng. 106 (1984) 187–192, https://doi.org/10.1115/1.3267578.

[20] S. Jamshed, S.R. Qureshi, M.S. Khalid, Numerical flow analysis and heat transfer in smooth and grooved tubes, in: 2016: pp. 163–174. https://doi.org/10.2495/AFM160141.

[21] M. Mohsenpour, M.-M. Pazuki, M. Salimi, M. Amidpour, Optimized heat exchanger network design for a phthalic anhydride plant using pinch technology: a Maximum Energy Recovery approach with economic analysis, Results. Eng. 24 (2024) 103438, https://doi.org/10.1016/j.rineng.2024.103438.

[22] K. Alawadhi, Y. Alhouli, A. Ashour, A. Alfalah, Design and optimization of a radial turbine to Be used in a rankine cycle operating with an OTEC system, J. Mar. Sci. Eng. 8 (2020) 855, https://doi.org/10.3390/jmse8110855.

[23] A. Bonar, A.D. Pasek, W. Adriansyah, R. Setiawan, Design and optimization of micro radial inflow turbine for low thermal organic rankine cycle using the preliminary design method, Results. Eng. 24 (2024) 103632, https://doi.org/10.1016/j.rineng.2024.103632.

[24] S. Hoseinzadeh, E. Assareh, A. Riaz, M. Lee, D.A. Garcia, Ocean thermal energy conversion (OTEC) system driven with solar-wind energy and thermoelectric based on thermo-economic analysis using multi-objective optimization technique, Energy Rep. 10 (2023) 2982–3000, https://doi.org/10.1016/j.egyr.2023.09.131.

[25] Z. Wu, H. Feng, L. Chen, W. Tang, J. Shi, Y. Ge, Constructal thermodynamic optimization for ocean thermal energy conversion system with dual-pressure organic rankine cycle, Energy Convers. Manage 210 (2020) 112727, https://doi.org/10.1016/j.enconman.2020.112727.

[26] M. Wang, R. Jing, H. Zhang, C. Meng, N. Li, Y. Zhao, An innovative Organic Rankine cycle (ORC) based Ocean Thermal Energy Conversion (OTEC) system with performance simulation and multi-objective optimization, Appl. Therm. Eng. 145 (2018) 743–754, https://doi.org/10.1016/j.applthermaleng.2018.09.075.

[27] F. Sun, Y. Ikegami, B. Jia, H. Arima, Optimization design and exergy analysis of organic rankine cycle in ocean thermal energy conversion, Appl. Ocean Res. 35 (2012) 38–46, https://doi.org/10.1016/j.apor.2011.12.006.

[28] N. Samsuri, N. Sazali, A.S. Jamaludin, M.N.M. Razali, Performance of ocean thermal energy conversion closed rankine cycle using different working fluids, in: IOP Conference Series: Materials Science and Engineering 1062, 2021 012040, https://doi.org/10.1088/1757-899X/1062/1/012040.

[29] F. Chen, L. Liu, J. Peng, Y. Ge, H. Wu, W. Liu, Theoretical and experimental research on the thermal performance of ocean thermal energy conversion system using the rankine cycle mode, Energy 183 (2019) 497–503, https://doi.org/10.1016/j.energy.2019.04.008.

[30] J. Gong, T. Gao, G. Li, Performance analysis of 15 kW closed cycle ocean thermal energy conversion system with different working fluids, J. Sol. Energy Eng. 135 (2013), https://doi.org/10.1115/1.4007770.

[31] T.C. Hung, S.K. Wang, C.H. Kuo, B.S. Pei, K.F. Tsai, A study of organic working fluids on system efficiency of an ORC using low-grade energy sources, Energy 35 (2010) 1403–1411, https://doi.org/10.1016/j.energy.2009.11.025.

[32] J.-I. Yoon, C.-H. Son, S.-M. Baek, H.-J. Kim, H.-S. Lee, Efficiency comparison of subcritical OTEC power cycle using various working fluids, Heat. Mass Transf. 50 (2014) 985–996, https://doi.org/10.1007/s00231-014-1310-8.

[33] K. Zhang, X. Lv, Y. Weng, Effect of working fluid on the ORC cycle performance of the ocean thermal energy conversion system, J. Phys. Conf. Ser. 2707 (2024) 012102, https://doi.org/10.1088/1742-6596/2707/1/012102.

[34] J.S. Brown, R. Brignoli, T. Quine, Parametric investigation of working fluids for organic rankine cycle applications, Appl. Therm. Eng. 90 (2015) 64–74, https://doi.org/10.1016/j.applthermaleng.2015.06.079.

[35] J. Peng, Y. Ge, F. Chen, L. Liu, H. Wu, W. Liu, Theoretical and experimental study on the performance of a high-efficiency thermodynamic cycle for ocean thermal energy conversion, Renew. Energy 185 (2022) 734–747, https://doi.org/10.1016/j.renene.2021.12.093.

[36] G.B. Monteiro, Exergetic, Thermodynamic Performance Optimization, and Analysis Of 100KW OTEC and Sotec Power Plants, Universidade Federal do Rio de Janeiro, 2024.

[37] S.M. Abbas, H.D.S. Alhassany, D. Vera, F. Jurado, Review of enhancement for ocean thermal energy conversion system, J. Ocean Eng. Sci. 8 (2023) 533–545, https://doi.org/10.1016/j.joes.2022.03.008.

[38] L. Aresti, P. Christodoulides, C. Michailides, T. Onoufriou, Reviewing the energy, environment, and economy prospects of Ocean Thermal Energy Conversion (OTEC) systems, Sustain. Energy Technol. Assess. 60 (2023) 103459, https://doi.org/10.1016/j.seta.2023.103459.

[39] A. Saadha, K.N. Ishihara, T. Ogawa, S. Basu, H. Okumura, Techno-economic analysis of combined onshore ocean thermal energy conversion technology and seawater air conditioning in small island developing states, Sustainability. 17 (2025) 4724, https://doi.org/10.3390/su17104724.

[40] A.G. Nickoloff, S.T. Olim, M. Eby, A.J. Weaver, Environmental impacts from the widespread implementation of ocean thermal energy conversion, Clim. Change 178 (2025) 102, https://doi.org/10.1007/s10584-025-03944-1.
[41] J.J. Cunningham, Z.E. Magdol, N.E. Kinner, Technical readiness of ocean thermal energy conversion (OTEC), Coast. Response Res. Cent. (2010) 246. http://coastalmanagement.noaa.gov/otec/docs/otectech1109.pdf.
[42] A.G. Nickoloff, S.T. Olim, M. Eby, A.J. Weaver, An assessment of ocean thermal energy conversion resources and climate change mitigation potential, Clim. Change 178 (2025) 103, https://doi.org/10.1007/s10584-025-03933-4.
[43] D. Vera, A. Baccioli, F. Jurado, U. Desideri, Modeling and optimization of an ocean thermal energy conversion system for remote islands electrification, Renew. Energy 162 (2020) 1399–1414, https://doi.org/10.1016/j.renene.2020.07.074.
[44] H. Semmari, D. Stitou, S. Mauran, A novel Carnot-based cycle for ocean thermal energy conversion, Energy 43 (2012) 361–375, https://doi.org/10.1016/j.energy.2012.04.017.
[45] H. Jiang, D. Jiang, L. Wang, D. Hua, Influence of ocean conditions on heat and mass transfer performance of heat exchangers: a review, Energy Sci. Eng. 13 (2025) 2164–2178, https://doi.org/10.1002/ese3.70022.
[46] N.-S. Cheng, Formulas for friction factor in transitional regimes, J. Hydraul. Eng. 134 (2008) 1357–1362, https://doi.org/10.1061/(ASCE)0733-9429(2008)134:9(1357).
[47] D. Bharathan, Staging Rankine Cycles Using Ammonia For OTEC Power Production, Golden, CO (United States), 2011. https://doi.org/10.2172/1010862.
[48] J. Frutiger, J. Andreasen, W. Liu, H. Spliethoff, F. Haglind, J. Abildskov, G. Sin, Working fluid selection for organic rankine cycles – Impact of uncertainty of fluid properties, Energy 109 (2016) 987–997, https://doi.org/10.1016/j.energy.2016.05.010.